Microtubules Remodel Actomyosin Networks in *Xenopus* Egg Extracts via Two Mechanisms of F-Actin Transport

Clare Waterman-Storer,* Devin Y. Duey,* Kari L. Weber,‡ John Keech,‡ Richard E. Cheney,‖ E.D. Salmon,¶ and William M. Bement‡§

*Department of Cell Biology and Institute for Childhood and Neglected Diseases, The Scripps Research Institute, La Jolla, California 92037; ‡Department of Zoology and §Program in Cellular and Molecular Biology, University of Wisconsin, Madison, Wisconsin 53706; and ‖Department of Cellular and Molecular Physiology and ¶Department of Biology, University of North Carolina, Chapel Hill, North Carolina 27599

Abstract. Interactions between microtubules and filamentous actin (F-actin) are crucial for many cellular processes, including cell locomotion and cytokinesis, but are poorly understood. To define the basic principles governing microtubule/F-actin interactions, we used dual-wavelength digital fluorescence and fluorescent speckle microscopy to analyze microtubules and F-actin labeled with spectrally distinct fluorophores in interphase *Xenopus* egg extracts. In the absence of microtubules, networks of F-actin bundles zippered together or exhibited serpentine gliding along the coverslip. When microtubules were nucleated from *Xenopus* sperm centrosomes, they were released and translocated away from the aster center. In the presence of microtubules, F-actin exhibited two distinct, microtubule-dependent motilities: rapid (~250–300 nm/s) jerking and slow (~50 nm/s), straight gliding. Microtubules remodeled the F-actin network, as F-actin jerking caused centrifugal clearing of F-actin from around aster centers. F-actin jerking occurred when F-actin bound to motile microtubules powered by cytoplasmic dynein. F-actin straight gliding occurred when F-actin bundles translocated along the microtubule lattice. These interactions required *Xenopus* cytosolic factors. Localization of myosin-II to F-actin suggested it may power F-actin zippering, while localization of myosin-V on microtubules suggested it could mediate interactions between microtubules and F-actin. We examine current models for cytokinesis and cell motility in light of these findings.

Key words: fluorescence microscopy • cytoplasmic dynein • myosin • cell motility • cytokinesis

Introduction

Cell division and directed cell motility in animal cells are the outcome of complex and dynamic interactions between the microtubule and actomyosin cytoskeletons. The relative roles of these two systems in cell division were apparent even before microtubules and actomyosin were recognized as ubiquitous components of eukaryotic cells, when Hiramoto showed that the mitotic spindle was necessary for establishment of the apparatus that drives cytokinesis, but was subsequently dispensable for cytokinesis itself (Hiramoto, 1956). Since that time, a wealth of studies based on micromanipulation, pharmacological perturbations, microscopy, and molecular genetics have established that a cortical contractile apparatus of filamentous actin (F-actin) and myosin-II powers animal cell fission, while microtubules are required for the proper assembly and positioning of that contractile apparatus (reviewed in Rappaport, 1996; Field et al., 1999).

Similar observations for cell locomotion date to the early 1970s. Cell locomotion involves the directed protrusion and subsequent adhesion of lamellipodia along the leading cell edge, and the concomitant retraction of the trailing cell edge. It is well established that disruption of the actin cytoskeleton prevents the protrusion of lamellipodia (e.g., Gail and Boone, 1971). However, microtubule poisons also decrease lamellipodial protrusion (Bershadsky et al., 1991; Waterman-Storer et al., 1999a), and result in loss of polarization such that protrusion occurs at random sites around the cell margin, halting cell locomotion

The online version of this article contains supplemental material.

Drs. Waterman-Storer and Bement contributed equally to this work.

Address correspondence to William M. Bement, Department of Zoology, University of Wisconsin, 1117 West Johnson St., Madison, WI 53706. Tel.: (608) 262-5683. Fax: (608) 262-9083. E-mail: wmbement@facstaff.wisc.edu or Clare Waterman-Storer, Department of Cell Biology, The Scripps Research Institute, 10550 N. Torrey Pines Rd., La Jolla, CA 92037. Tel.: (858) 784-9764. Fax: (858) 784-9779. E-mail: waterman@scripps

(Vasiliev et al., 1970; Goldman, 1971). Thus, microtubules both promote actin-based lamellipodial protrusion and provide the vector for its placement (reviewed in Waterman-Storer and Salmon, 1999).

As yet, however, the interrelationships between microtubules and actomyosin are poorly understood. Several reports have described proteins that bind to both microtubules and F-actin (e.g., Griffith and Pollard, 1978; Goode et al., 1999; reviewed in Goode et al., 2000). Additionally, a number of pharmacological studies have documented that microtubules somehow regulate actomyosin-based contractility (Danowski, 1989; Kolodney and Elson, 1995; Enomoto, 1996), actomyosin-dependent cortical flow (Edds, 1993; Canman and Bement, 1997), actomyosin purse string assembly and closure (Bement et al., 1999), and actin-based lamellipodial activity (Bershadsky et al., 1991; Waterman-Storer et al., 1999a). Nevertheless, the basic principles of microtubule-actomyosin interactions have remained elusive. The technological difficulties inherent in understanding such interactions are formidable, in that both microtubules and F-actin are abundant and highly dynamic, and the processes of cell division and lamellipodial protrusion occur rapidly, and within narrow windows of space and time. Further, microtubule and F-actin–based motility can result from both changes in polymer dynamics as well as motor protein-dependent translocation (reviewed in Inoue and Salmon, 1995).

Thus, many critical questions posed about the nature of microtubule-actomyosin interactions have gone unanswered. For example, it is unknown whether microtubules modulate the actomyosin cytoskeleton directly (i.e., by physical association with, and exertion of force upon actomyosin) or indirectly (i.e., by interaction with and transport of signaling molecules or organelles that themselves control actomyosin). It is also unknown how different spatial arrays of microtubules differentially affect the actomyosin cytoskeleton. The latter question is especially important with respect to complex processes such as cytokinesis and cell locomotion. Cytokinetic furrow establishment in both echinoderm embryos (Rappaport, 1996) and cultured cells (e.g., Rieder et al., 1997; Savoian et al., 1999) is signaled by paired, astral arrays of microtubules, while directed cell locomotion is generally associated with a forward-facing microtubule organizing center and microtubule plus ends facing the direction of migration (Gotlieb et al., 1981).

We recently developed *Xenopus* egg extracts as a model system for studying microtubule and F-actin interactions (Sider et al., 1999). In that study, we found evidence that F-actin associates with microtubules in unfixed, static specimens. Here, we have exploited the extract system to analyze the dynamics of microtubule-F-actin interactions using time-lapse dual-wavelength digital fluorescence microscopy (Waterman-Storer and Salmon, 1997) and fluorescent speckle microscopy (FSM[1]; Waterman-Storer et al., 1998, 1999b). Using these methods, we can examine the relationship of cytoskeletal filaments labeled with distinct fluorescent probes and distinguish motility events driven by cytoskeletal polymerization from those driven by motor-based movement. The results show that microtubules form physical contacts with and exert force on F-actin bundles to remodel F-actin networks in specific, predictable ways. Further, we find two distinct types of microtubule-dependent F-actin motion, one in which F-actin rides as a passenger on motile microtubules, and one in which F-actin moves along the lattice of microtubules. We also show that these microtubule/F-actin interactions require cytosolic factors and have a profound influence on the spatial disposition of F-actin. Finally, we demonstrate that this influence is dependent on the organization of microtubules and upon the activity of the microtubule motor, cytoplasmic dynein.

[1]*Abbreviations used in this paper:* BDM, butane 2,3 monoxime; DE-DIC, digitally enhanced differential interference contrast; FSM, fluorescent speckle microscopy; MAP, MT-associated protein; MT, microtubule; MTOCs, microtubule-organizing centers.

Materials and Methods

Materials

Porcine brain tubulin was purified by rounds of polymerization and depolymerization and labeled with succinimidyl ester of X-rhodamine (Molecular Probes) and stored at ~35 mg/ml at –80°C in injection buffer (50 mM K-glutamate, 0.5 mM KCl, pH 7.0; see Waterman-Storer and Salmon, 1997). Chicken breast muscle actin was purified from acetone powder and labeled with succinimidyl ester of Oregon green (Molecular Probes) as described in Waterman-Storer et al. (2000) and stored at ~4 mg/ml in G-Buffer (2 mM Tris, 0.2 mM $CaCl_2$, 0.2 mM ATP, 0.5 mM β–mercaptoethanol [BME]) at –80°C. Alexa 488-conjugated phalloidin was purchased from Molecular Probes. *S. purpuratus* axoneme fragments were prepared as in Bell et al. (1982) and stored at a protein concentration of ~100 mg/ml at –80°C until use. CHO cell centrosomes, purified as described (Mitchison and Kirschner, 1986), were the kind gift of Drs. Tom Keating and Gary Borisy (University of Wisconsin, Madison). Rat brain kinesin, the kind gift of Dr. Sher Karki (University of Pennsylvania, Philadelphia) was isolated as the 9s fraction from sucrose gradients of the ATP-eluate of brain microtubules. Purified rabbit skeletal muscle G-actin was the kind gift of Dr. Velia Fowler (The Scripps Research Institute). Rabbit skeletal muscle α-actinin was purchased from Cytoskeleton, Inc. Mouse anti-cytoplasmic dynein intermediate chain mouse monoclonal antibody 70.1 (Steuer et al., 1990; Sigma-Aldrich) was concentrated into PBS and used at 2 mg/ml in the extract.

Preparation of Interphase Xenopus Egg Extracts

Interphase *Xenopus* egg extracts were prepared as described in Sider et al. (1999). In brief, eggs were collected from adult *Xenopus* females, washed four to six times in 1× MMR (10 mM NaCl, 0.2 mM KCl, 0.1 mM $MgCl_2$, 0.2 mM $CaCl_2$, 0.01 mM EDTA, and 0.5 mM Hepes, pH 7.8) and stored at 16°C for 1–3 h. Eggs were dejellied in 1× MMR containing 2% cysteine (pH 7.8), and then rinsed four times in 0.25× MMR. Eggs were then rinsed two times in ice-cold ELB buffer and two times in ice-cold ELB containing 10 μg/ml pepstatin, leupeptin, chymostatin, aprotinin, and 1 mM Pefabloc (Boehringer). After transfer to clear ultracentrifuge tubes, eggs were packed by centrifugation for 1 min in a clinical centrifuge, excess buffer was removed, and the protease inhibitors and cycloheximide were added to final concentrations of 10 and 100 μg/ml, respectively. Eggs were crushed by centrifugation for 20 min at 20,000 *g* in an SW41 rotor at 4°C. The yellow cytoplasmic layer was removed with a syringe bearing a 19-gauge needle, aliquoted into 50-μl aliquots, and frozen in liquid N_2. Aliquots were stored at –80°C until use.

Preparation of Demembranated Sperm

Male *Xenopus* were anesthetized in MS222 (Sigma), and their testes were removed. Testes were rinsed three times in ice-cold MBSH (110 mM NaCl, 2 mM KCl, 1 mM $MgSO_4$, 0.5 mM $NaPO_4$, 2 mM $NaHCO_3$, and 15 mM Tris-base, pH 7.6) and then macerated in 4 ml of ice-cold HSPPP (250 mM sucrose, 1 mM EDTA, 0.5 mM spermidine, 0.2 mM spermine, 15 mM Hepes pH 7.4, 10 μg/ml pepstatin, leupeptin, chymostatin, aprotinin, and 1 mM Pefabloc). After filtering through cheesecloth, samples were pelleted in a clinical centrifuge at 4°C, resuspended in 1 ml HSPPP containing 500 μg/ml lysophosphatidylcholine (Boehringer) and incu-

bated 5 min at room temperature. Samples were then diluted in 10 ml HSPPP containing 0.3% BSA, pelleted, resuspended in HSPPP-BSA, repelleted, resuspended in HSPPP containing BSA and 30% glycerol, frozen in liquid N_2, and stored at –80°C.

Specimen Preparation for Dynamic Imaging

To image microtubule and F-actin dynamics in *Xenopus* egg extracts, a 50-μl aliquot of extract was thawed, experimental components were added, and the sample was stored on ice for up to 2 h until imaging. X-rhodamine tubulin was added to the extract at 0.1 mg/ml and Oregon green actin or Alexa 488 (AX-488) phalloidin (Molecular Probes) was added at 0.1 mg/ml or 0.148 μM, respectively. We noted no major differences in F-actin behavior regardless of whether AX-phalloidin or OG-actin was used as a probe. For fluorescent speckle imaging of microtubules, X-rhodamine–labeled tubulin was added at 10–50 μg/ml to the extract. To reduce fluorescent photobleaching and photodamage, Oxyrase (Oxyrase Inc.) was added to the extracts to a concentration of 0.3–0.6 U/ml (Waterman-Storer and Salmon, 1997).

Xenopus egg extracts containing experimental components were imaged in sealed slide/coverslip chambers. Coverslips were coated with casein to reduce the nonspecific binding of labeled proteins to the coverslip surface. This was done by placing 5 μl of 10% casein in water in the center of the coverslip and spinning it dry on a modification of the device described in Inoue (1986). To form the imaging chamber, 1–1.5 μl of ice-cold extract were put on a precleaned slide (Clay-Adams) and a casein-coated coverslip was placed on the drop, the extract was allowed to spread, and was sealed on all sides with valap (1:1:1 mixture of vaseline/lanolin/paraffin). This resulted in a layer of extract that was 3–7 μm thick and which was rapidly warmed to room temperature via its contact with the glass.

To image the interactions between purified motile microtubules and F-actin bundles, perfusion chambers were assembled with a coverslip placed on two strips of double-stick tape spaced ~2–4 mm apart on a slide. The chamber was coated with rat brain kinesin for 10 min, washed three times with PEMTA (100 mM Pipes, 1 mM EGTA, 2 mM $MgSO_4$, 10 μM taxol, and 1 mM ATP), one time with PEMTA containing 10% casein, and a final time with PEMTA. Then, a mixture of 22 μM rabbit skeletal muscle G-actin, 0.4 μM AX-488 phalloidin, 4.1 μM rabbit skeletal muscle α-actinin, 0.3 μM X-rhodamine speckled, taxol stabilized microtubules (assembled from 99.5% unlabeled tubulin, 0.5% labeled tubulin as described in Waterman-Storer and Salmon, 1998) in 7.2 mM Pipes, 4.6 mM Tris, 3.3 mM NaCl, 0.3 mM $MgSO_4$, 0.07 mM $CaCl_2$, 0.14 mM EGTA, 0.8% sucrose, 0.16% dextran, 1.4 μM taxol, 0.16 mM β-mercaptoethanol, 0.7 mM dithiothreitol, 0.2 mM ATP, pH ~7 were added to the chamber, which was sealed with VALAP and transferred immediately to the microscope stage for imaging.

Digital Fluorescence Imaging and FSM

Time-lapse digital images of Oregon green–labeled actin or Alexa 488 phalloidin and/or X-rhodamine–labeled tubulin in extracts were acquired using the multimode digital imaging system described in Salmon et al. (1998) with excitation filters for X-rhodamine (570 nm) and Alexa 488 or Oregon green (490 nm). Shutter and filterwheel timing and position were controlled by MetaMorph software (Universal Imaging Corp.). For dual-wavelength time-lapse imaging, pairs of images of F-actin and microtubules were collected at 8–15-s intervals with a lag of ~1 s between images within a pair.

The interactions of pure motile microtubules with pure F-actin bundles were imaged using a Nikon TE-300 Quantum microscope equipped with an Ultraview (Perkin Elmer) dual spinning disk real-time confocal scanner. This allowed for clear imaging of fluorescent microtubules and F-actin at the coverslip surface in the 70-μm-thick perfusion chambers. Illumination was provided by a 50 mW Kr/Ar laser (Melles Griot) coupled to the confocal head by a optical fiber (Point Source), passed through an electronic filterwheel (Sutter Instruments) with excitation filters for Oregon green (488 nm) and X-rhodamine (568) and through a polychromatic mirror and focused onto the specimen with a 100× 1.4 NA Plan Apo DIC objective. Emission from the specimen collected by the objective was reflected off the polychromatic mirror through a polychromatic emission filter and confocal images were collected with a Hamamatsu Orca II cooled CCD camera using the 14-bit slow scan mode. Shutter and filterwheel timing and position were controlled by MetaMorph software (Universal Imaging Corp.).

Images of fluorescent sperm asters in fixed extracts were also collected on the TE-300 Quantum using the Orca II camera, but the confocal scanner was removed. Widefield epi-illumination was provided by a HBO-100W mercury arc lamp and excitation wavelength was selected with an electronic filterwheel (Ludl Biopoint) containing filters for Oregon green (490 nm) and X-rhodamine (570 nm), and a triple bandpass dichromatic mirror and emission filter for DAPI/FITC/X-rhodamine (Chroma). Shutter and filterwheel timing and position were controlled by a Ludl controller and MetaMorph software (Universal Imaging Corp.).

Image Processing and Data Analysis

All position, length, and intensity measurements on digital images were made using the analysis functions of the MetaMorph software. Distances in images were calibrated from images of a 10-μm stage micrometer. For velocity measurements, the positions of fiduciary marks in polymers were tracked in successive frames of time-lapse series using the track points function in Metamorph. This function calculates instantaneous velocities for the distance moved during the interval between successive frames and exports the values into Microsoft Excel 97 for analysis. To determine the average number of microtubules emanating from the centrosome, microtubules were counted at 2-min intervals for the first 4 min of the imaging period and averaged. For the quantification of F-actin bundle network alignment, a total of seven experiments (four control and three nocodazole) were selected based on similarity in length (minimum of 10 min) and time-lapse interval (15 s). Hard copies were made of every 10th frame, and the number of intersections of three or more actin bundles was counted. Because the number of intersections varied among the different time-lapse series, numbers were expressed as percents of starting intersection number.

To determine the dynamic relation between F-actin and microtubules, RGB color overlays of time-lapse series of F-actin and speckled microtubules were made and viewed as movie series. To make color overlays, the average intensity of all images in each time-lapse series was equalized by multiplication by a constant (using the equalize light function in Metamorph). The F-actin series was then color-coded green and the microtubule series was color-coded red (using the color encode function in Metamorph) and they were combined into a single RGB series. In some cases, the images were processed as described in Waterman-Storer and Salmon (1998). Quicktime movies of time-lapse series of images were assembled using Adobe Premier as described in Waterman-Storer et al. (1997).

Fixation of Extracts and Immunofluorescence Analysis of Extracts

To examine sperm aster formation in solution, 3 μl of extract containing 0.4 μM X-rhodamine tubulin and demembranated sperm was incubated at room temperature in a microcentrifuge tube. Extracts were then fixed by addition of an equal volume of 40 mM Pipes, 0.5 mM $MgCl_2$, 0.5 mM EGTA, 20 μM taxol, 50% glycerol, and 1.85% formaldehyde, pH 6.9. To test the involvement of cytoplasmic dynein in sperm aster expansion, anti-cytoplasmic dynein intermediate chain antibody 70.1 was added to the extract at 0.7 mg/ml. 1.25 μl of fixed extract was pressed between a slide and coverslip, the preparation was sealed with VALAP and was imaged. For immunofluorescent localization of myosins, extracts were processed as described previously (Mandato et al., 2000). In brief, 1.5 μl extract was flattened between two coverslips, incubated 15 min at room temperature and then plunged into liquid nitrogen. The coverslips were pried apart, placed in room temperature fixative (1 mM $MgCl_2$, 5 mM EGTA, 80 mM K-Pipes, pH 6.8, 0.2% Triton X-100, 3.7% paraformaldehyde, 0.25% glutaraldehyde, and 0.5 mM taxol) for 5 min. Samples were quenched for 10 min in PBS containing 100 mM $NaBH_4$, blocked two times for 5 min in 1× TBS + 0.1% NP-40 + 5 mg/ml BSA (TBSN-BSA), and incubated for 15 min at 37°C in a moist chamber in TBSN-BSA containing DM1A mouse anti-tubulin (1:250; ICN Biomedicals), affinity-purified rabbit anti–*Xenopus* myosin-IIA or -IIB (10 μg/ml; Kelley et al., 1996) and Alexa 488 phalloidin (1 U/ml) or rabbit anti–chick brain myosin-5 (10 μg/ml) and Alexa 488 phalloidin. Samples were washed four times for 5 min in TBSN-BSA with gentle agitation and then incubated for 15 min at 37°C in rhodamine anti-mouse (1:100; Organon Teknika-Cappel) and Cy5–anti-Rabbit (1:100; Molecular Probes). Samples were washed four times for 5 min in TBSN-BSA with gentle agitation, mounted in 80% glycerol containing 20 mM *N*-propylgallate. Images were collected on a Biorad 1024 laser scanning confocal on a Zeiss Axiovert microscope equipped with a 63× 1.4 NA Plan Apo objective lens in the Department of Zoology (University Wisconsin). Illumination was provided by a 50 mW Kr/Ar laser and fluorescence was detected with three photomultiplier tubes.

Supplemental Materials

Quicktime videos to accompany many of the figures are available at http://www.jcb.org/cgi/content/full/150/2/361/DC1.

Results

To define the basic principles governing microtubule/F-actin interactions in cytoplasm, either Alexa 488–labeled phalloidin (Alexa 488 phalloidin) or Oregon green–labeled actin (Oregon green actin) was added to interphase-arrested, crude *Xenopus* egg extracts for visualizing F-actin, along with X-rhodamine tubulin for visualizing microtubules. Thin (~3–7 μm) preparations of extracts were then analyzed in sealed slide/coverslip chambers at room temperature by dual-wavelength time-lapse digital fluorescence microscopy and FSM. We first characterized the behavior of each cytoskeletal polymer independent of the other one, and then analyzed the dynamic interactions between microtubules and F-actin.

F-Actin Exhibits Zippering Alignment and Serpentine Gliding in the Absence of Microtubules

The dynamic behavior of F-actin was analyzed in the absence of microtubules by performing time-lapse imaging

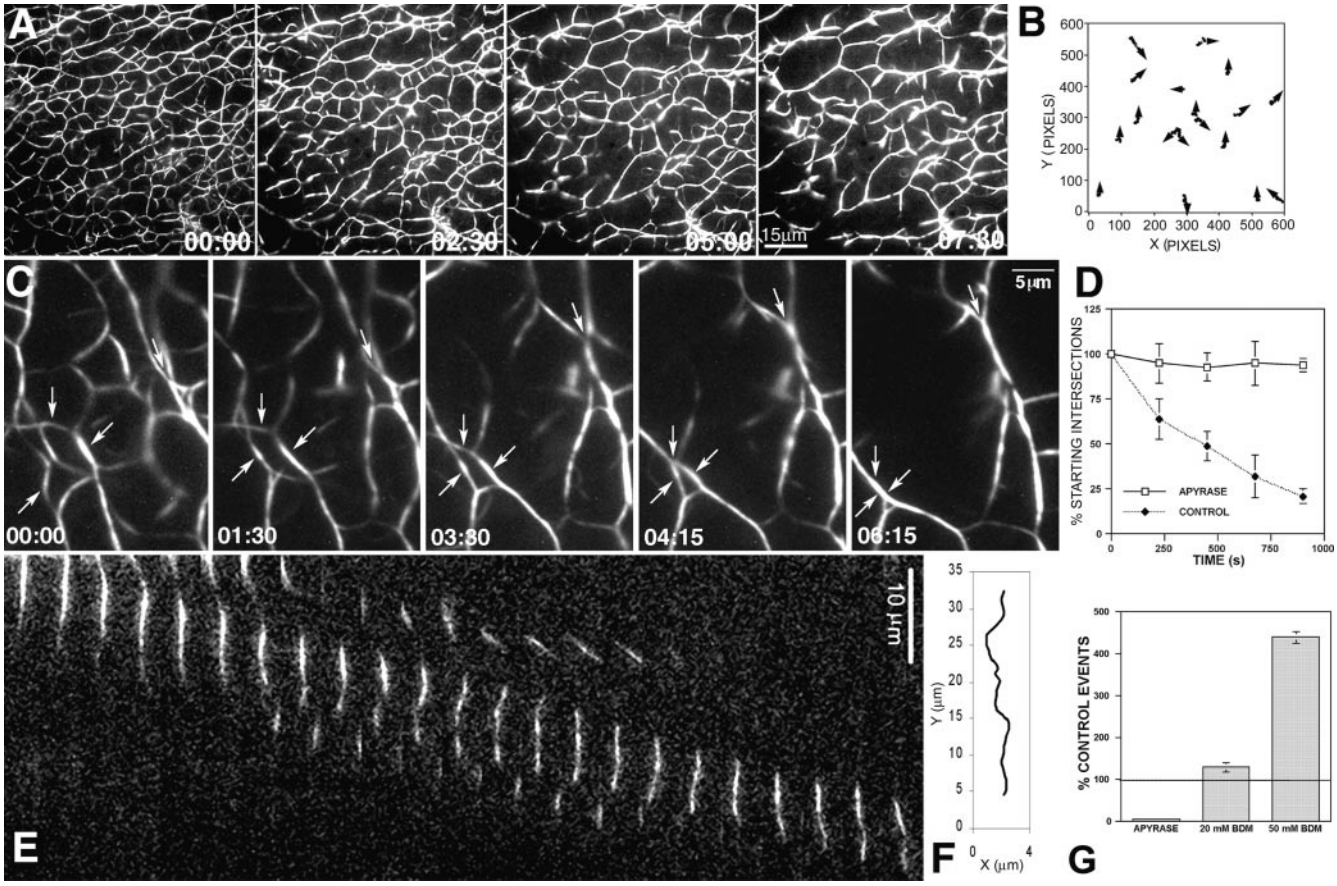

Figure 1. Microtubule-independent F-actin motility in *Xenopus* egg extracts. (A) Low magnification, time-lapse view of an Alexa 488 phalloidin-stained F-actin network formed in the presence of nocodazole (10 μM). The number of F-actin bundles decreases and their thickness increases over time as bundle zippering results in annealing of adjacent bundles. (B) Trajectory plot of the position of F-actin bundles in a time-lapse series of 600 × 600 pixel images. Time points are separated by 15 s; arrowheads indicate the direction of movement in final frame. Most of the bundles move only short distances and display no consistent direction of movement. (C) High magnification, time-lapse view of F-actin bundle zippering. Adjacent bundles (arrows) zipper together at intersections, resulting in the formation of larger bundles and a decrease in the number of intersections. (D) Depletion of ATP by apyrase treatment (10 μg/ml) of extracts blocks F-actin zippering. The number of intersections between adjacent F-actin bundles was quantified in extracts at various times after the initiation of imaging in the absence (control) and presence (apyrase) of apyrase. In the absence of apyrase, the number of intersections decreases over time; in the presence of apyrase the number of intersections fails to decrease and the networks did not change over time. Data shown are mean ± SEM; $n = 2$. (E) High magnification, time-lapse view of F-actin bundle serpentine gliding. The F-actin bundle moves sinuously across the substrate. Images in successive panels were acquired at 15-s intervals. (F) Plot of the X-Y coordinates of the point of peak fluorescence intensity of the F-actin bundle shown in E. This demonstrates the serpentine path followed by the F-actin bundle. (G) Serpentine gliding is prevented by depletion of ATP with apyrase and is stimulated by BDM. The number of gliding events per field of view in samples subjected to the indicated treatment was compared with the number of events in control samples from the same experiment. Apyrase almost completely eliminated serpentine gliding. BDM at 20 mM had a slight stimulatory effect, while BDM at 50 mM more than tripled the number of bundles moving by serpentine gliding. Data shown are mean ± SEM; $n = 2$. Time is in min/s. Also see supplemental videos 1–3 at http://www.jcb.org/cgi/content/full/150/2/361/DC1.

of labeled F-actin in extracts containing 10 μM nocodazole to prevent tubulin polymerization. Similar results were achieved in the absence of nocodazole, but in areas of the sample chamber that lacked microtubules. In both cases, the absence of microtubules in the field of view was confirmed by imaging in the X-rhodamine channel. Under these conditions, F-actin assembled into an interconnected network of bundles (Fig. 1 A and video 1), and exhibited two kinetically and morphologically distinct types of motility that we term zippering and serpentine gliding.

Zippering resulted from slow (0.044 ± 0.010 μm/s; Table I) coalescence and bundling together of two or more adjacent F-actin bundles within the network (Fig. 1, A–C, video 2), such that over 10–15 min, the number of intersections between network bundles and the total number of network bundles decreased (Fig. 1 D), while the size of bundles and the area of the spaces between adjacent bundles in the network increased. The motion of F-actin bundles during zippering generally occurred perpendicular to the axis of the bundle, but was randomly directed relative to other bundles within network, as indicated by maps of the trajectories of F-actin bundles over time (Fig. 1 B). The decrease in the number of intersections between bundles resulting from zippering was prevented by ATP-depletion via apyrase treatment (Fig. 1 D) implying the involvement molecular motor proteins. We tested the sensitivity of zippering to the myosin ATPase inhibitor, butane 2,3 monoxime (BDM; Cramer and Mitchison, 1995). However, BDM promoted conversion of networks into isolated bundles that subsequently underwent serpentine gliding (see below), making it impossible to determine if BDM inhibited zippering.

Serpentine gliding was specific to areas of the preparation where network formation was incomplete and F-actin was present as relatively thin, isolated bundles. In these areas, portions of the bundles occasionally broke away and glided unidirectionally across the coverslip surface in a curvilinear, serpentine fashion at 0.111 ± 0.012 μm/s (Fig. 1, E and F, video 3; Table I). Like zippering, serpentine gliding was prevented by apyrase treatment (Fig. 1 G). Serpentine gliding was not inhibited by BDM but in fact was stimulated by it, particularly at higher BDM concentrations (Fig. 1 G). Because most of the gliding F-actin was wider than the limit of resolution of the light microscope (240 nm for green fluorescence), at least some of the serpentine gliding represented movement of bundles of F-actin rather than individual F-actin filaments.

In addition to zippering and serpentine gliding, F-actin was also occasionally observed to form comet-like structures (see Online Supplemental Material and Table I). These comets were most frequently observed near microtubule-organizing centers (MTOCs) and likely formed as a result of actin nucleation off of membrane vesicles (Ma et al., 1998; Moreau and Way, 1998).

Microtubules Exhibit Gliding and Astral Expansion on Coverslips and in Solution

We next characterized the behavior of microtubules in extracts containing either 10 μM cytochalasin D or 5 μM latrunculin A to inhibit actin filament formation. Previous work has documented basic features of microtubule polymerization dynamics and microtubule-based motility in *Xenopus* extracts (Belmont et al., 1990; Allan and Vale, 1991; Waterman-Storer et al., 1995), so only those aspects of microtubule motility relevant to this study will be described. When microtubules were either polymerized from MTOCs provided by demembranated *Xenopus* sperm (Fig. 2, A and B) or spontaneously polymerized in the extract (not shown), they underwent directed movement along the coverslip surface at 0.306 ± 0.061 μm/s (Fig. 2 A, video 4; Table I). These rates are similar to known rates of microtubule translocation in both *Xenopus* extracts (Belmont et al., 1990) and intact cells (Keating et al., 1997). Extract microtubules also displayed dynamic instability polymerization/depolymerization dynamics (not shown, Belmont et al., 1990; Waterman-Storer et al., 1995), and such microtubules can appear to translocate via treadmilling (Rodionov and Borisy, 1997; Waterman-Storer and Salmon, 1997). However, time-lapse FSM (Waterman-Storer et al., 1998, 1999b) revealed that fiduciary marks on microtubules moved relative to the substrate (Fig. 2 A, video 4), demonstrating that microtubules were translocating rather than treadmilling. Microtubules moved with their plus ends leading, as judged by following microtubules released from demembranated sperm MTOCs (Fig. 2 A) or nucleated from sea urchin axoneme fragments (not shown; Paschal and Vallee, 1987).

The polymerization of microtubules followed by their release from sperm MTOCs resulted in centrifugal expansion of microtubule asters (Fig. 2 B, video 5). During expansion, individual microtubules, as well as radially organized groups of 5–10 microtubules, were released and translocated away from the aster center (Fig. 2 B). This re-

Table I. Velocity Analysis for F-Actin and Microtubule Movements in Interphase Xenopus Egg Extracts

Structure/Movement	Condition	Velocity*	Measurements	Events measured	Experiments
		μm/s			
Zippering F-actin cable	10 μM nocodazole	0.044 ± 0.010	438	24	8
Serpentine gliding F-actin cable	10 μM nocodazole	0.111 ± 0.012	404	25	5
F-actin comet	250 μM orthovanadate	0.096 ± 0.011	192	17	2
Microtubules gliding on coverslip	Random microtubules	0.306 ± 0.061	448	50	16
Jerking F-actin cable	Random microtubules	0.289 ± 0.030	430	36	16
Jerking F-actin cable	Sperm aster microtubules	0.258 ± 0.024	437	46	11
F-actin gliding on microtubules	Random microtubules	0.050 ± 0.021	73	3	2

*Expressed as mean ± SEM.

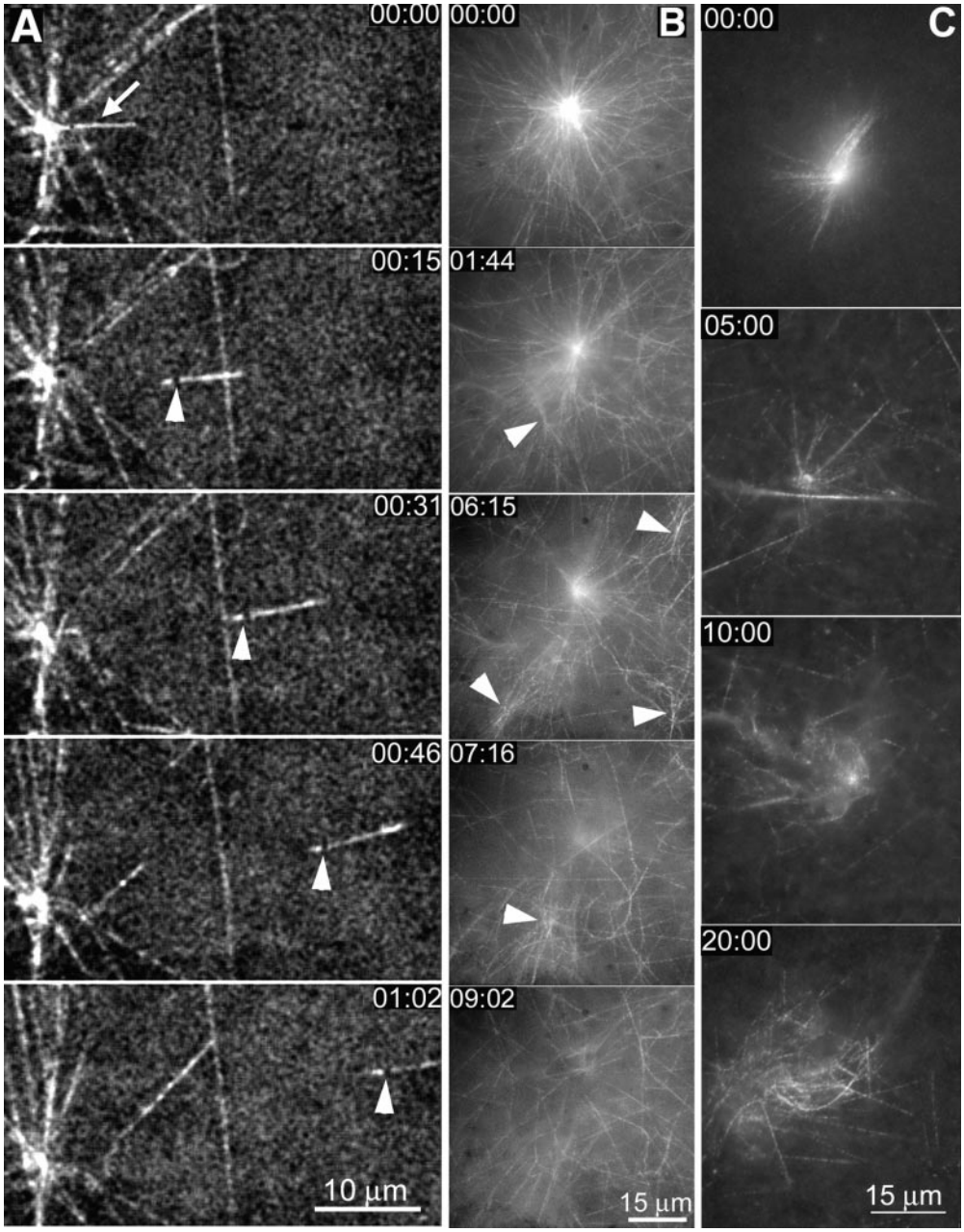

Figure 2. Microtubule gliding and aster expansion in *Xenopus* egg extracts. (A) FSM of astral microtubule release and gliding along the substrate. The microtubule nucleated at the aster center (arrow) grows several microns and is then released at its minus end from the aster. The dark gap (arrowhead) in the speckled microtubule moves relative to the substrate demonstrating that the microtubule is translocating away from the aster via the action of a minus end–directed motor on the coverslip. (B) Low magnification, time-lapse view showing expansion of a sperm aster. Immediately after the initiation of imaging, the aster is well organized into a radial array containing many microtubules. Over time, microtubules are released and translocate away from the aster, and small radial arrays of microtubules (arrowheads) wander away from the original aster. (C) Low magnification, images of asters that were formed by adding demembranated sperm to extracts in solution and fixed at the time point shown and then placed in a slide-coverslip chamber. At the earliest time point, asters are well focussed, similar to those observed in thin preparations (see B). At the 5-min time point, asters have expanded, and the microtubules do not extend from a single, well-defined point. At 10- and 20-min time points, expansion and disorganization is even more pronounced. Time is in min/s. Also see supplemental videos 4 and 5 at http://www.jcb.org/cgi/content/full/150/2/361/DC1.

sulted in the disassembly of the asters over 10–20 min. This astral expansion also occurred on the same time course for microtubule asters formed in solutions of extracts that were fixed at various times after the addition of demembranated sperm and examined later in slide/coverslip (Fig. 2 C). This indicates that aster expansion was not merely an artifact of the close apposition of microtubule asters to a microtubule motor-coated coverslip, but that coverslips act as surrogate sites for motor attachment that are normally provided by membranous organelles, microtubules, or other structures that are present in extracts in solution.

Microtubules Remodel F-Actin Networks

We next analyzed the effect of microtubules on the behavior and organization of F-actin in extracts. To achieve this, F-actin dynamics were first analyzed by time-lapse fluorescence microscopy in areas of the preparation that exhibited randomly arrayed microtubules. In the presence of microtubules, F-actin bundles still formed networks and exhibited zippering alignment. However, superimposed on the zippering was a new motility unlike any observed in the absence of microtubules. Specifically, F-actin displayed a morphologically and kinetically distinct jerking

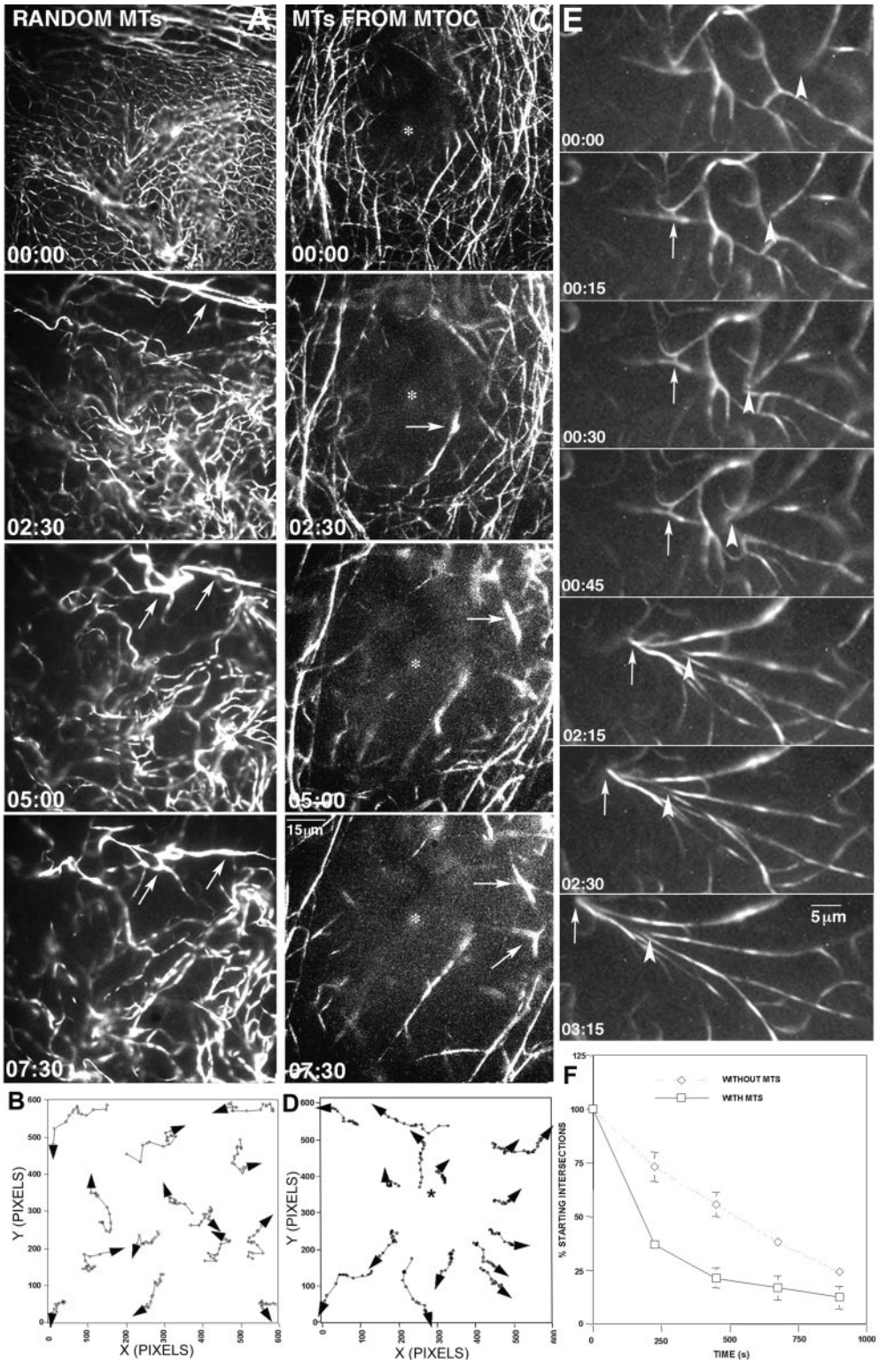

Figure 3. Microtubules remodel F-actin networks by rapid jerking of F-actin bundles. (A) Low magnification, time-lapse view of an F-actin network formed in the presence of randomly arrayed microtubules. An F-actin bundle network forms and undergoes zippering, but is also subject to rapid jerking movements that grossly distort the organization of the network. (B) Trajectory plot of the position of F-actin bundles in a time-lapse series of 600 × 600 pixel images in the presence of randomly arrayed microtubules. Individual bundles move long distances, but do not move in any consistent direction, and change direction rapidly. Time points are separated by 15 s; arrowheads indicate the direction of movement in final frame. (C) Low magnification, time-lapse view of an F-actin network formed in the presence of microtubules organized by a demembranated sperm MTOC (position marked by an asterisk). The F-actin network undergoes zippering, but is progressively cleared centrifugally from the area occupied by the MTOC. Over time, thick actin bundles (arrows) accumulate around the periphery of the MTOC. (D) Trajectory plot of F-actin bundle motility in the presence of aster-organized microtubules. Individual bundles move long distances, in a consistently centrifugal direction out from the position of the MTOC center (asterisk). Time points are separated by 15 s; arrowheads indicate the direction of movement in final frame. (E) High magnification, time-lapse view of part of an F-actin network subjected to jerking motility in the presence of randomly arrayed microtubules. An F-actin bundle (arrowhead) making up one branch of the network undergoes directed movement (0:00–00:30) and collides with an adjacent bundle (at 00:30) forming a V-shaped junction between the bundles. The junction then undergoes a change in trajectory (time 00:45) and rapidly moves in unison with a neighboring bundle (arrow; 02:15–03:15). The movement brings the moving bundles into collisions with other bundles. (F) Microtubules accelerate the bundling of F-actin networks. The number of intersections between F-actin bundles within a network was quantified at various time after the initiation of imaging in four control experiments in the presence of microtubules (with MTs) and three experiments using extract containing 10 μM nocodazole (without MTs). The presence of microtubules accelerates the rate of bundling relative to the rate of bundling in their absence, as judged by the more rapid decrease in the number of intersections. To control for variation in the number of starting intersections, results are expressed as the % of the starting number of intersections. Results shown are mean ± SEM. Time is in min/s. Also see supplemental videos 6–8 at http://www.jcb.org/cgi/content/full/150/2/361/DC1.

motion (Fig. 3). The jerking motility of F-actin bundles was characterized by rapid, often discontinuous movements (Fig. 3, A, B, and E, videos 6 and 8). Quantification of the movements revealed that in the presence of microtubules, jerking F-actin occurred at 0.289 ± 0.030 μm/s (Table I). This was ~7.5 and ~3 times faster than rates for either F-actin zippering motion or serpentine gliding motility seen in the absence of microtubules, respectively (Table I). The jerking motility grossly disrupted F-actin networks (Fig. 3 A), as F-actin bundles were pushed and pulled into V shapes and then pushed and pulled into each other (Fig. 3 E). Upon collision, F-actin bundles coalesced into larger bundles, thus increasing the rate at which the F-actin bundles in the networks zippered together and aligned (Fig. 3 F).

Demembranated sperm were then added to the extract and actin behavior was examined in relation to an astral microtubule array. In this case, distortion of the F-actin network and rapid jerking movements of the F-actin bundles were again observed, but they occurred in a distinct pattern. Specifically, F-actin moved in a jerking motion centrifugally from the sperm aster center outward, resulting in a rapid clearing of F-actin from the area immediately surrounding the aster (Fig. 3, C and D, video 7). The speed of F-actin jerking movement was 0.258 ± 0.024 μm/s, similar to that seen in samples containing randomly oriented microtubules (Table I). However, in contrast to F-actin observed in the presence of randomly arrayed microtubules, wherein F-actin accumulated in disordered bundles (Fig. 3 A), the clearing of F-actin from around sperm asters resulted in the accumulation of bundles oriented circumferentially around the periphery of the aster (Fig. 3 C).

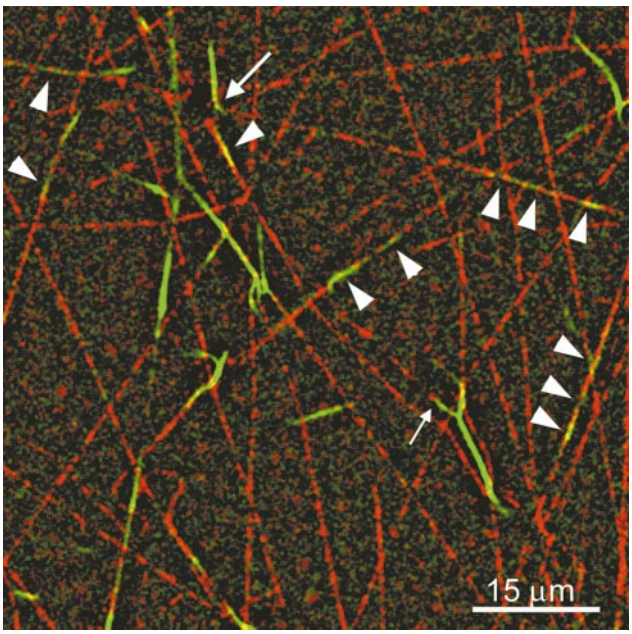

Figure 4. F-actin bundles form lengthwise associations with microtubules. Double label images of microtubules obtained from time-lapse movies were digitally processed to remove the background of unpolymerized fluorescent label in the extract, color encoded, and combined into an RGB overlay to reveal the codistribution of the two polymers. Microtubules are randomly arrayed on the coverslip surface. Some F-actin is not associated with microtubules, but a substantial amount is aligned lengthwise along microtubules (arrowheads). Occasionally, ends of F-actin bundles terminate on the side of microtubules (large arrow) and microtubule and F-actin bundles can associate end-to-end (small arrow).

F-Actin Jerking Is Caused by Cytoplasmic Dynein-dependent Microtubule Movement Pushing and Pulling on F-Actin Bundles

The observed F-actin jerking motility was similar in velocity to microtubule gliding, strongly suggesting that microtubules and F-actin were physically interacting. To test this notion, dual-wavelength digital fluorescence microscopy was used to determine whether microtubules and F-actin directly associated with one another in the extracts. In samples with randomly arrayed microtubules, this analysis revealed that F-actin bundles often exhibited extensive lengthwise associations with microtubules (Fig. 4, arrowheads). In some cases, F-actin bundles terminated at a contact along the shaft or at the tip of a microtubule (Fig. 4, arrows).

We next examined the basis of microtubule-dependent F-actin jerking motility using time-lapse microtubule FSM in conjunction with time-lapse digital fluorescence microscopy of F-actin. Movie series of time-lapse microtubule FSM and F-actin made into RGB overlays revealed that both the spatial pattern and the rate of movement of jerking F-actin bundles mirrored the pattern and rate of the movement of speckles on the lattice of translocating microtubules with which the F-actin was in contact (Fig. 5, A–D, video 9). In addition, pauses in F-actin movement were correlated with pauses in microtubule movement. Similarly, when demembranated sperm were added to the extracts, F-actin moved outward away from microtubule aster centers while remaining bound to translocating microtubules (Fig. 5 E, video 10). These results demonstrate that F-actin can bind to and ride as a passenger on motile microtubules.

The finding that microtubules in the extracts moved along the coverslip with plus ends leading suggested that microtubule translocation and F-actin jerking was powered by a minus end–directed motor, such as cytoplasmic dynein (Paschal and Vallee, 1987). To test this hypothesis, we added 0.25 mM sodium orthovanadate to the extracts, or 2 mg/ml anti-cytoplasmic dynein intermediate chain antibody 70.1 (Steuer et al., 1990). These treatments have been shown to inhibit cytoplasmic dynein-mediated organelle motility (Allan and Vale, 1991; Verde et al., 1991) and mitotic spindle pole formation in *Xenopus* extracts (Walczak et al., 1998), respectively. Both treatments inhibited microtubule gliding, release, and translocation from sperm asters, as well as sperm aster expansion and fragmentation (Fig. 6, A and B). However, neither treatment blocked the microtubule nucleating activity of sperm asters. As a result, the sperm asters became huge, with >150 microtubules per aster (Fig. 6 A, video 11; Table II). Similar results were obtained when cytoplasmic dynein was inhibited during sperm aster formation in solution (Fig. 6 B), indicating that cytoplasmic dynein acts to move microtu-

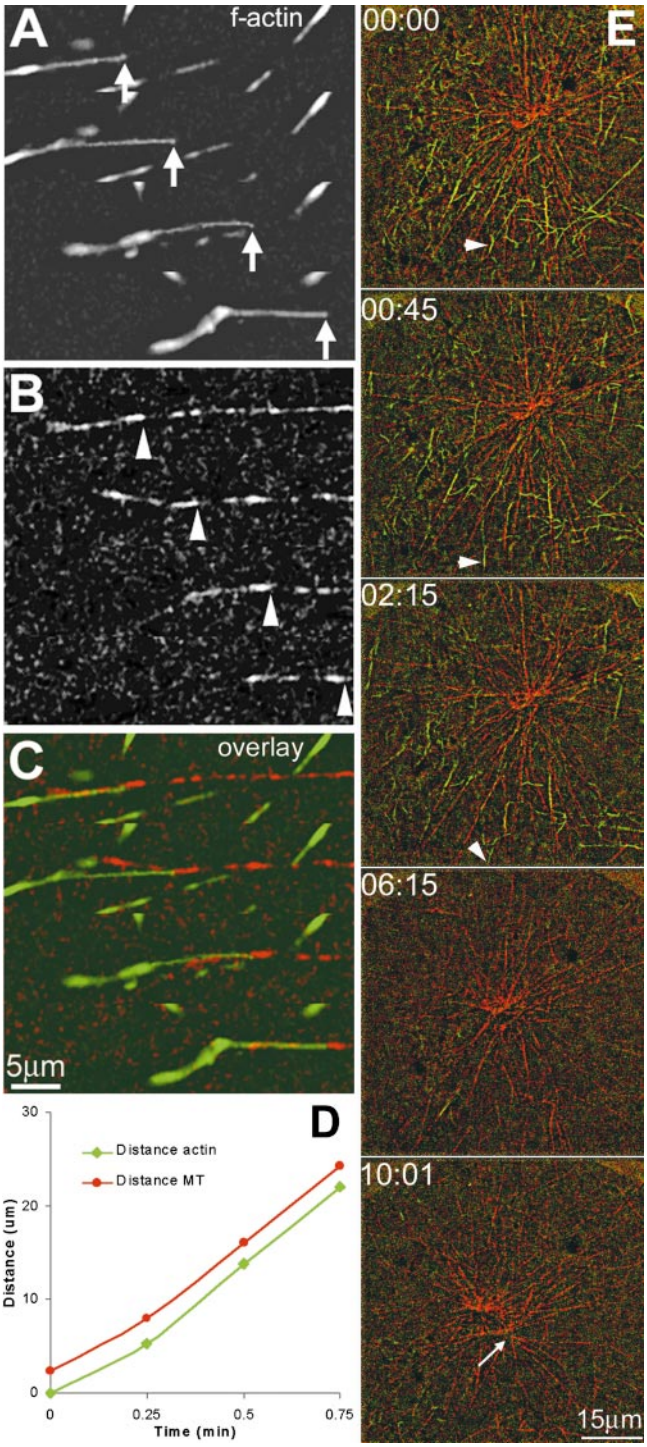

Figure 5. F-actin jerking results from F-actin binding to translocating microtubules. (A) Time-lapse views of an F-actin bundle (arrow) that undergoes jerking motility. (B) Time-lapse, FSM views of the microtubule associated with the F-actin bundle in A. That this microtubule is gliding is demonstrated by movement of the boundary between a dark region and a fluorescent spot on the lattice of the speckled microtubule (arrowhead). (C) Dual-wavelength fluorescence imaging of actin (green) and tubulin (red) showing the combined images depicted in A and B. The images were digitally processed to reduce the background, color-coded, and combined into an RGB overlay to reveal the codistribution of the two polymers. The movement of the F-actin bundle mirrors the movement of the speckled microtubule, indicating that the F-actin is attached to the lattice of the gliding microtubule. Images in A–C were acquired at 15-s intervals. (D) Plot of the distance of the tip (arrow in A) of the F-actin bundle and the speckle mark (arrowhead in B) on the microtubule from the origin (the position of the F-actin bundle tip at time 0:00) vs. time. The plot shows the exact correspondence in the movement of the two polymers. (E) Centrifugal clearing of F-actin around a sperm aster. Demonstrated by dual-wavelength fluorescence imaging of X-rhodamine tubulin (red) and Alexa 488 phalloidin labeling of F-actin (green) in *Xenopus* egg extracts. Time in min/s. F-actin is extensively aligned along astral microtubules (times 00:00–6:15). Over time, F-actin bundles are translocated away from the sperm aster center (arrowheads, times 00:00–2:15) while remaining bound to microtubules are released and translocate away from the aster as the aster fragments (arrow) and expand (time 10:01, arrow). Also see supplemental videos 9 and 10 at http://www.jcb.org/cgi/content/full/150/2/361/DC1.

Table II. Microtubule Behavior for Different MTOCs in Interphase Xenopus Egg Extracts

MTOC	Rate of microtubule release	Microtubules/ centrosome
Sperm aster (n = 7, 53.3 min)	3.6 min	87.0 ± 33.5
Sperm aster, 2 mg/ml anti-dynein (n = 4, 53.3 min)	0/min	>150
CHO centrosome (n = 7, 62.6 min)	0.21/min	26.7 ± 6.7

bules while either bound to the coverslip or to other sites in the extract.

Both anti-cytoplasmic dynein antibodies (Fig. 6, A and D) and orthovanadate (Fig. 6 D) inhibited microtubule-dependent F-actin jerking movements and centrifugal clearing of F-actin from around sperm asters, demonstrating that F-actin jerking motility is ultimately powered by cytoplasmic dynein-dependent movement of translocating microtubules. Neither antibody treatment nor vanadate affected either F-actin zippering (Fig. 6 E) or serpentine gliding (not shown). However, vanadate treatment promoted formation of F-actin comets, consistent with previous work (see online supplemental material; see Frischknecht et al., 1999).

As an alternative approach to confirm the requirement for microtubule release and translocation in F-actin jerking motility and clearing from around MTOCs, centrosomes isolated from CHO cells were added to extracts and F-actin movement around these MTOCs was monitored. In contrast to sperm MTOCs, CHO cell centrosomes rarely release microtubules (Table II). Accordingly, F-actin exhibited very infrequent jerking motility and was not cleared from around CHO centrosomes (not shown).

F-Actin Straight Gliding Is Due to Movement of F-Actin Bundles along Stationary Microtubules

Careful analysis of dual-wavelength microtubule FSM and F-actin RGB overlays surprisingly revealed a second form of microtubule-dependent, F-actin motility that was much less dominant and less obvious than F-actin jerking. We

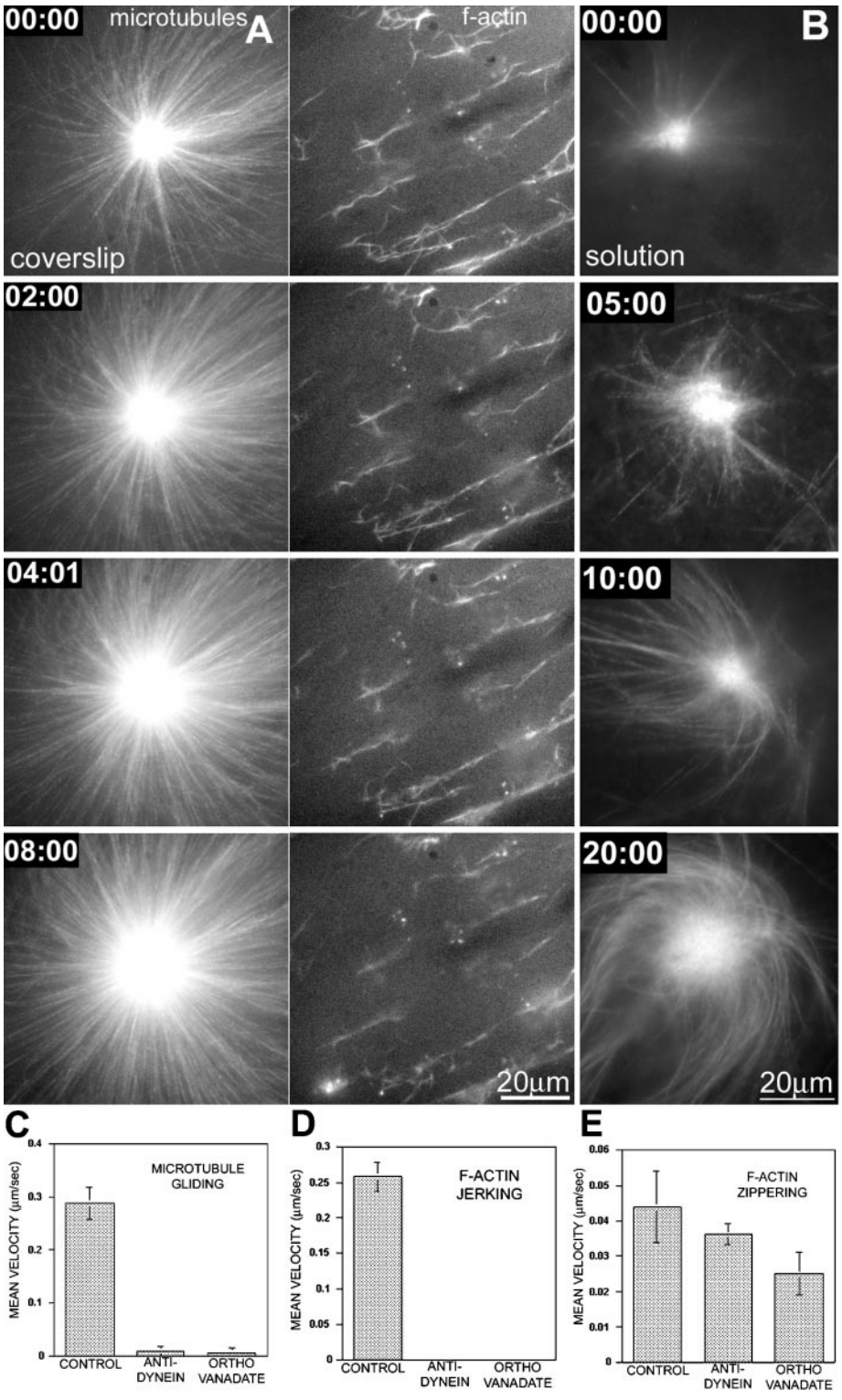

Figure 6. Cytoplasmic dynein powers microtubule gliding, aster expansion, and F-actin bundle jerking. (A) Low magnification, time-lapse views of microtubules (left) seeded from a demembranated *Xenopus* sperm and F-actin (right) in the presence of 2 mg/ml anti-cytoplasmic dynein intermediate chain antibody 70.1. The antibody inhibits the translocation of microtubules away from the MTOC, thus inhibiting aster expansion but does not inhibit microtubule nucleation and growth, thus inducing a striking accumulation of microtubules (left; compare to Fig. 2 B). The antibody also inhibits F-actin jerking and prevents centrifugal clearing of F-actin from the aster (right). Time is in min/s. (B) Low magnification views showing asters that were fixed at various times after the addition of demembranated sperm to *Xenopus* extracts in solution in the presence of 2 mg/ml anti-cytoplasmic dynein intermediate chain antibody 70.1. In the presence of the antibody, even at late time points, the aster remains tightly focussed and has many microtubules emanating from it (compare to Fig. 2 C). (C) Cytoplasmic dynein activity is required for microtubule gliding. Quantification of the rate of microtubule gliding across the substrate was calculated in control extracts (n = 11), extracts containing 2 mg/ml 70.1 (n = 9), and extracts containing 250 μM sodium orthovanadate (n = 5). Inhibition of cytoplasmic dynein drastically slowed the rate of microtubule gliding. (D) Cytoplasmic dynein activity is required for F-actin jerking. Quantification of the rate of F-actin jerking was determined from the same experiments used for C. Inhibition of cytoplasmic dynein with 70.1 antibodies or orthovanadate completely eliminated F-actin jerking. (E) Cytoplasmic dynein is not required for F-actin zippering. Quantification of the rate of F-actin zippering was determined from the same experiments used for C. Cytoplasmic dynein inhibition with 70.1 antibodies or orthovanadate does not affect F-actin zippering. Also see supplemental video 11 at http://www.jcb.org/cgi/content/full/150/2/361/DC1.

termed this motility straight gliding, as it was characterized by F-actin moving slowly (0.050 ± 0.021 μm/s; Table I) along a nearly straight or gently arched course (Fig. 7, video 12). F-actin bundles observed to be undergoing straight gliding motility actually moved unidirectionally relative to fluorescent speckles on the lattice of microtubules that remained stationary with respect to the substrate (Fig. 7, video 12, Table I). Although the straight gliding and serpentine gliding motilities of F-actin occurred at similar rates, they could easily be visually distinguished by their path of movement, as demonstrated by kinetic analysis of their trajectories (compare Fig. 7 D with Fig. 1 F), and straight gliding never occurred in the absence of microtubules. However, F-actin straight gliding

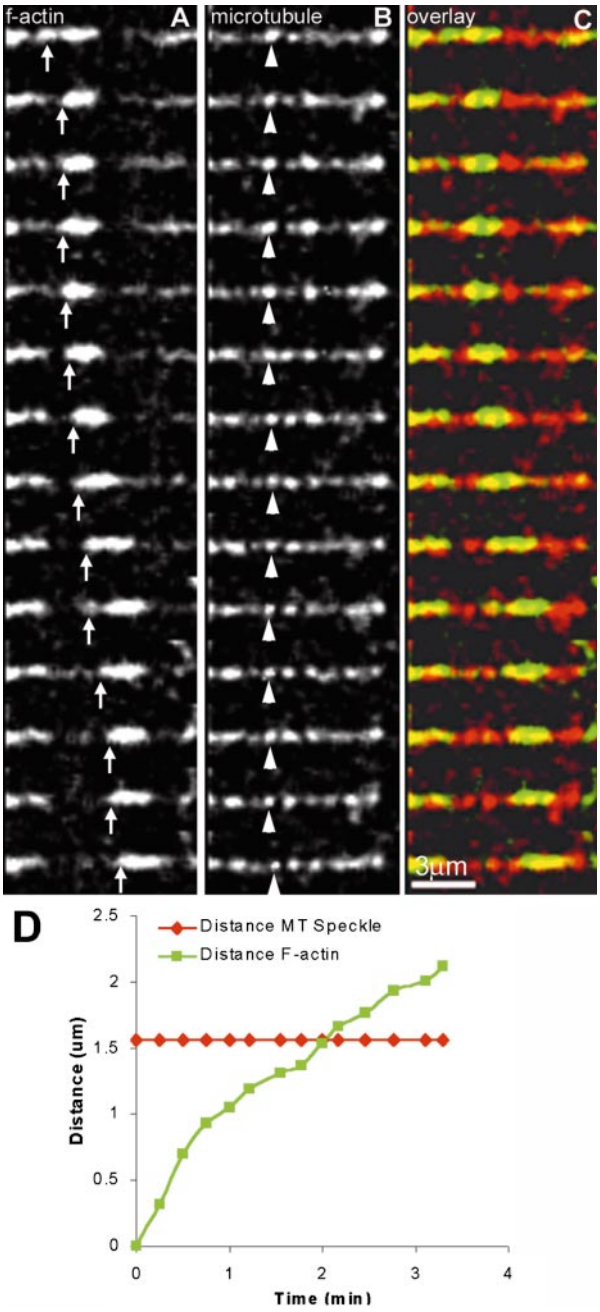

Figure 7. F-actin can translocate along the lattice of stationary microtubules. (A) Time-lapse fluorescence imaging shows F-actin moving in a straight path. (B) Time-lapse FSM view of a stationary microtubule in the same field of view shown in A. The speckle mark indicated by the arrowhead does not move with respect to the substrate, showing that this microtubule is stationary throughout the period of imaging. (C) Color overlay of F-actin from A and the microtubule from B shows that the F-actin moves with respect to the stationary speckle marks on the microtubule lattice. Images in A–C were acquired at 15-s intervals (also see supplemental video 12 at http://www.jcb.org/cgi/content/full/150/2/361/DC1). (D) Plot of the distance of the tip (arrow in A) of the F-actin bundle and the speckle mark on the microtubule (arrowhead in B) from the origin (the position of the F-actin bundle tip at time 0:00) vs. time. This demonstrates that the F-actin moves relative to the microtubule lattice.

along microtubules was difficult to unambiguously identify unless the microtubules were stationary, a situation that was quite infrequent. Thus, we could not determine the directionality of F-actin movement along microtubules emanating from sperm asters, presumably due to the high rate of microtubule release and translocation and the rapidity of F-actin clearing from the region surrounding the aster. Efforts to immobilize microtubules by coating coverslips with tubulin antibodies or motor-inactive kinesins were frustrated by the tendency of such manipulations to cause the formation of extensive microtubule bundles, while efforts to test the effects of BDM on this motility were frustrated by the tendency of BDM to cause microtubule disassembly in extracts. Nevertheless, these results demonstrate that F-actin bundles can use the microtubule lattice as a substrate for motility.

Microtubule-dependent F-Actin Motility Is Specific and Requires Cytosolic Proteins

It could be argued that the observed translocation of F-actin bundles by moving microtubules results from nonspecific interactions between the two polymer systems. To test this possibility directly, we labeled purified rabbit skeletal muscle F-actin with Alexa 488 phalloidin and cross-linked it into bundles by adding purified rabbit skeletal muscle α-actinin at an ~5:1 molar ratio. To this we added taxol-stabilized, fluorescent speckled microtubules assembled from purified porcine brain tubulin (99.5%) and X-rhodamine–labeled tubulin (0.5%) in a buffer containing ATP. This mixture was then added to a slide/coverslip chamber that was previously coated with rat brain kinesin to power the motility of the taxol stabilized microtubules along the coverslip. Under these conditions, F-actin formed bundles of similar thickness as those spontaneously formed in the extracts, but did not exhibit zippering, serpentine gliding or comet formation. In addition, microtubules exhibited gliding along the coverslip surface at 0.69 ± 0.086 μm/s (4 experiments, 277 measurements on 23 microtubules), as expected for brain kinesin (Vale et al., 1985). In spite of the motility of microtubules, the F-actin bundles did not undergo jerking or straight gliding motility (Fig. 8). Further, time-lapse dual-wavelength confocal analysis revealed that motile microtubules would often contact multiple F-actin bundles without causing any perturbation of the position of the bundles (Fig. 8 and video 13). These results demonstrate that the interaction between motile microtubules and F-actin bundles is specific and dependent on *Xenopus* cytosolic factors.

Myosin-V Localizes along Extract Microtubules

To probe the mediator of the interactions between microtubules and F-actin, two approaches were taken. First, we assessed the potential role of membranous organelles as linkers between microtubules and F-actin using multimode fluorescence and digitally enhanced differential interference contrast (DE-DIC) microscopy (Allan and Vale, 1991; Waterman-Storer et al., 1995; Salmon et al., 1998). However, no evidence was found for DIC-refractile membranous organelles linking the F-actin bundles to microtubules (not shown). In separate experiments nonionic detergents were added to extracts to further test the role of

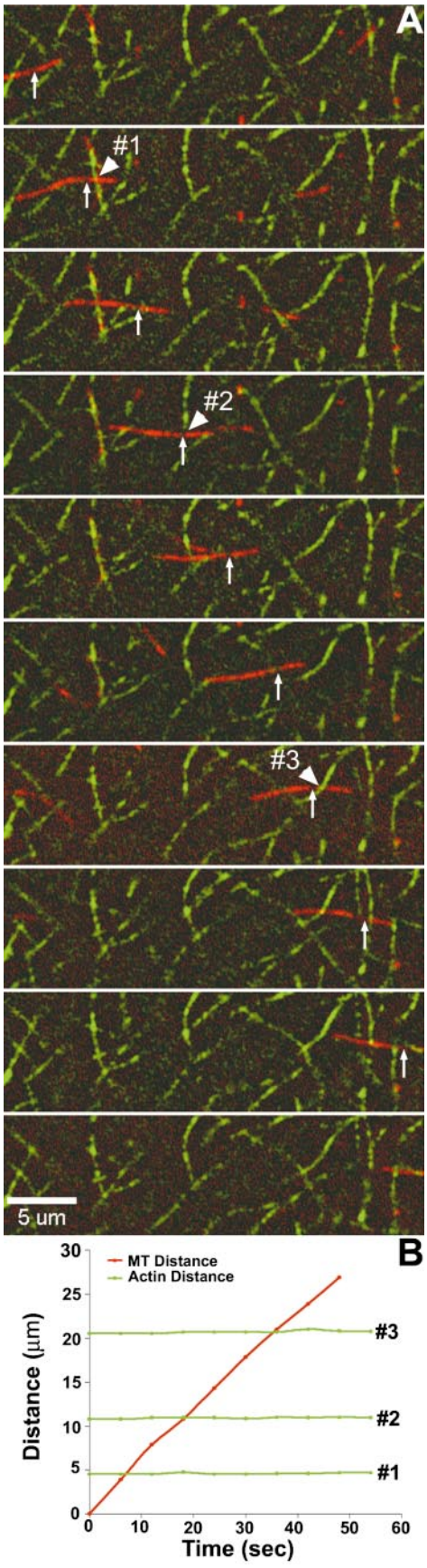

Figure 8. Translocating microtubules fail to transport F-actin in the absence of extract factors. (A) Time-lapse, dual-label fluorescence views of Alexa 488 phalloidin–labeled skeletal muscle F-actin/alpha actinin bundles (green) and microtubules (red) assembled from 99.5% porcine brain tubulin and 0.5% X-rhodamine–labeled tubulin that are gliding across a coverslip coated with rat brain kinesin. A microtubule translocates across the field of view, as judged by following the translocation of its speckle mark (arrow). En route, it makes contact with multiple F-actin bundles, three of which are indicated (#1–3). In spite of these multiple contacts, the moving microtubule does not transport any F-actin bundles. (B) Plot of the distance of the microtubule speckle mark (arrow in A) and of the three different F-actin bundles indicated in A (#1–3) from the origin (position of the speckle at time 00:00) vs. time. This demonstrates that the contact with the microtubule doesn't change the position of the actin bundles. Also see supplemental video 13 at http://www.jcb.org/cgi/content/full/150/2/361/DC1.

membranes in mediating microtubule F-actin interactions, however, this prevented microtubule polymerization, presumably due to release of calcium from membrane-bound compartments.

We then used immunofluorescence of fixed extracts to assess the role of candidate myosin motors in the interaction between microtubules and F-actin. Rapidly frozen extract samples were analyzed for the distribution of myosin-IIA, which in interphase culture cells localizes to microtubules when F-actin is depolymerized, and during mitosis localizes to spindle microtubules (Kelley et al., 1996). Triple-label analysis demonstrated that myosin-IIA was predominantly associated with F-actin bundles (Fig. 9 A) as was myosin-IIB (not shown). We then used a simlar approach to analyze the localization of myosin-V, an actin-based motor that has been shown to associate with microtubules and mitotic spindles in vivo (Espreafico et al., 1998; Wu et al., 1998). In striking contrast to myosin IIA, myosin-V was distributed in punctae that aligned extensively along microtubules as well as sometimes on the coverslip surface (Fig. 9 B).

Discussion

In this study, we have systematically analyzed microtubule and F-actin motility in cell-free lysates of *Xenopus* eggs. We first established the dynamic properties of these systems in isolation of one another, and then characterized for the first time the direct dynamic interactions between the two systems to define the basic modes for microtubule/F-actin interactions in cytoplasm. Our results define two distinct types of motile microtubule/F-actin interactions: one in which F-actin rides as a passenger on cytoplasmic dynein-powered motile microtubules, and a second, less dominant form in which F-actin moves along the microtubule lattice. These interactions are specific, and require *Xenopus* cytosolic factors. We show that as a result of these interactions, microtubules remodel F-actin networks. Below, we discuss the novel cytoskeletal motilities described in this study, their possible molecular mechanisms, and how the basic modes of interaction between microtubules and F-actin may have implications for the mechanisms of cytokinesis and cell motility.

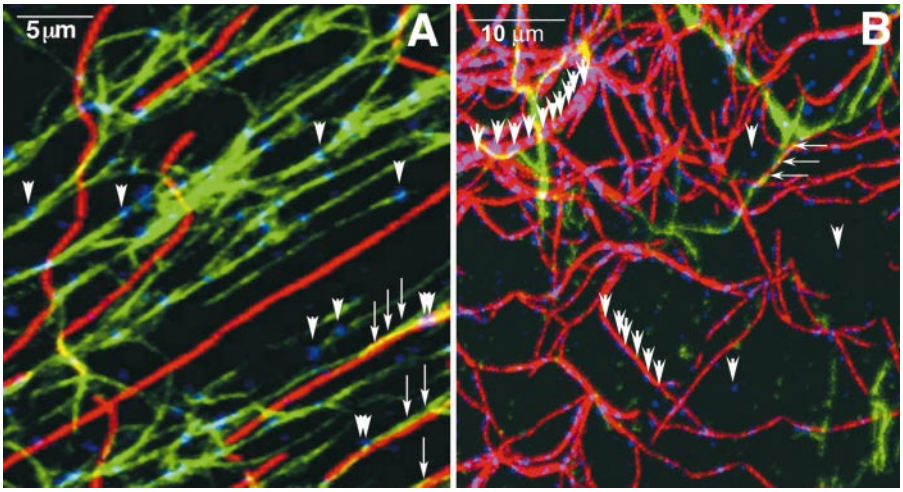

Figure 9. Localization of myosin-IIA and -V in *Xenopus* egg extracts. (A) Triple label fluorescence analysis of myosin-IIA (blue), microtubules (red), and F-actin (green) in rapidly frozen extracts. Myosin-IIA punctae (arrowheads) are found predominantly on F-actin bundles. In some regions, myosin-2, microtubules, and F-actin are colocalized (triple arrowheads); in other regions, F-actin and microtubules are colocalized in the absence of myosin-2 (arrows). (B) Triple label fluorescence analysis of myosin-V (blue), microtubules (red), and F-actin (green) in rapidly frozen extracts. Most of the myosin-V (arrowheads) is found on microtubules or the substrate. In both A and B colocalization of red, blue and green result in white.

Microtubule-dependent F-Actin Motilities

Two distinct forms of microtubule-dependent F-actin motility were observed in *Xenopus* extracts: F-actin jerking and F-actin straight gliding. Simultaneous analysis of F-actin and fiduciary-marked microtubules by FSM showed that the rapid jerking movement of F-actin paralleled the movement of an associated microtubule, indicating that F-actin was bound to a translocating microtubule. F-actin jerking was cytoplasmic dynein dependent. In this case, the role of cytoplasmic dynein in translocating F-actin is likely to be indirect: F-actin is statically cross-linked and riding as a passive passenger on cytoplasmic dynein-driven motile microtubules. However, our results do not rule out the possibility that cytoplasmic dynein or its interacting partner, dynactin, may also cross-link F-actin to microtubules. The dynactin complex binds to cytoplasmic dynein, microtubules, and the actin-binding protein, spectrin, and contains both the actin-related protein Arp-1 (centractin) as well as conventional actin (reviewed in Karki and Holzbaur, 1999). This provides a multitude of scenarios for linking actin to microtubules. However, in our studies it was difficult to tell if cytoplasmic dynein antibodies inhibited the binding of F-actin to microtubules, because we could not differentiate whether F-actin bundles were actively bound or passively intersecting with microtubules unless the microtubules were moving and distorting the F-actin network.

In addition to cytoplasmic dynein, recent studies have uncovered several nonneuronal candidates for static MT/actin cross-linking proteins (reviewed in Goode et al., 2000). These include MIP-90, a HeLa cell MT-associated protein (MAP) that localizes to actin structures and binds actin in vitro (Gonzalez et al., 1998), a yeast homologue of the actin-binding protein, coronin, that contains a MT-binding domain (Goode et al., 1999), calponin, an actin-, tropomyosin-, and calmodulin-binding protein in smooth muscle that binds tubulin in vitro (Fujii et al., 1997), or one of the plakins, some of which have been found to bind both microtubules and F-actin (Karakesisoglou et al., 2000). MTs and F-actin could also be indirectly coupled via the protein, plectin, which can link both actin and MTs to intermediate filaments (Svitkina et al., 1996).

We have also observed the gliding of F-actin bundles along stationary microtubules. However, observation of this type of motility was rare. This motility could only be unambiguously demonstrated when both F-actin and microtubules were sparse, microtubules were stationary and optimally speckled, and F-actin bundles were relatively small, thin, and not exhibiting other forms of motility. Because F-actin gliding along microtubules was observed in the presence of phalloidin, monomer treadmilling seems unlikely. We therefore suspect that this activity is mediated by one or more motor proteins. This could occur by three mechanisms: (a) a bifunctional motor complex of a myosin motor and a microtubule motor translocating on either/both polymers, (b) a microtubule motor bound statically to F-actin and translocating on the microtubule lattice, or (c) a myosin motor bound statically to microtubules and producing force along F-actin. Recent evidence indicating that kinesin can bind to myosin-V (Huang et al., 1999) together with the localization of myosin-V along microtubules that we observed in *Xenopus* extracts, makes kinesin/myosin-V a strong candidate for a bifunctional microtubule–F-actin motor complex. With its ability to translocate on microtubules and possibly bind to actin, cytoplasmic dynein/dynactin is a possible candidate for the second model. Finally, myosin-VI has been reported to associate with the microtubule-binding protein, CLIP-170 (Lantz and Miller, 1998), suggesting that a myosin bound to the microtubule via CLIP-170 could power F-actin movement.

Microtubule-dependent F-Actin Motilities and Cytoskeletal Remodeling In Vivo

Our analysis has revealed that not only do both short- and long-term microtubule–F-actin interactions occur, they have a profound impact on the organization of the F-actin cytoskeleton. While F-actin networks spontaneously form and align in the absence of microtubules in the extracts, microtubule-dependent F-actin jerking pushes F-actin bun-

dles into each other, promoting the assembly of F-actin into larger bundles. In addition, the pattern of F-actin movement in the presence of microtubules depends on the arrangement of the microtubules. When microtubules are nucleated from and organized by a sperm MTOC, release and transport of astral microtubules results in F-actin being cleared outward from the MTOC. The combined action of F-actin zippering and microtubule-dependent pushing of F-actin bundles into each other generates the formation of large bundles around the perimeter of the MTOC. However, in the absence of a defined MTOC, while large F-actin bundles are still created by zippering and accelerated by microtubule-based pushing, the distribution of these bundles does not have any particular spatial pattern.

The observation that the final outcome of the interaction between microtubules and F-actin is critically dependent on the organization of the microtubules is striking in light of several decades of studies showing that proper assembly of the actomyosin cytokinetic apparatus is critically dependent on the apposition of two asters some minimum distance apart (reviewed in Rappaport, 1996; Field et al., 1999). The finding that F-actin is transported outward and accumulates at the aster periphery on microtubules that are released and translocate away from the centrosome provides one relatively simple explanation for these observations. Specifically, we would predict that two adjacent sperm asters transporting F-actin centrifugally would generate an especially heavy accumulation of F-actin in the area between them. Further, the tendency of F-actin to zipper into bundles and of microtubules to increase the rate of F-actin bundling would drive a positive feedback loop for actomyosin accumulation in areas between asters. Although this astral ejection model is based on our results in vitro, it is consistent with several in vivo observations including the directed transport of F-actin toward the incipient cytokinetic furrow (e.g., Cao and Wang, 1990; Bao, Y., and D.J. Fishkind. 1999. *Mol. Biol. Cell.* 10:263a), the transport of cortical F-actin away from repositioned microtubule organizing centers (Hird and White, 1993; Benink et al., 2000) and the sensitivity of cytokinesis to manipulations which perturb areas between asters (see Rappaport, 1996). Thus, it would be interesting to monitor ejection and translocation of microtubules from spindle poles in dividing cells to determine if it occurs during cytokinesis, as it does during interphase in a variety of cells (see below, Keating et al., 1997; Waterman-Storer et al., 1997)

The findings of this report also provide insight into the means by which microtubules and F-actin interact during cell locomotion. It is well established that F-actin nucleation occurs at the leading edge of migrating cells (reviewed in Mitchison and Cramer, 1996), making it unlikely that F-actin is translocated to the leading edge as a passenger on microtubules. However, recent studies show that microtubule movement and organization in locomoting cells may be mediated by cytoplasmic dynein (Yvon and Wadsworth, 1999a). Thus, cytoplasmic dynein-based microtubule movements could drive the bundling and zippering of F-actin into graded polarity actin bundles present in migrating cells (Cramer et al., 1997). In addition, we have previously shown that microtubules in the lamella of migrating cells exhibit retrograde flow towards the cell center in an actomyosin-dependent fashion. This suggests that microtubules and F-actin are cross-linked to one another in vivo, which could be mediated by the same cross-linker that binds F-actin to motile microtubules in extracts in the present study. This observation further implies that in motile cells, actomyosin contractility may be dominant over microtubule/cytoplasmic dynein motion, and that the links between microtubules and F-actin may result in actomyosin remodeling of microtubule arrays. Finally, microtubules have been observed to target to focal adhesions at the leading edge of locomoting cells and promote the dissolution of the contacts (Kaverina et al., 1998, 1999). This phenomenon also could rely on the cross-linking or gliding of microtubules along focal adhesion-associated F-actin.

Novel Behaviors of F-Actin and Microtubules

Underlying the microtubule-dependent F-actin motility in *Xenopus* egg extracts were two novel forms of microtubule-independent F-actin motility: zippering of F-actin bundles and serpentine gliding of F-actin along the coverslip surface. Although zippering has not been described previously, it is predicted by classic cortical flow models (e.g., Bray and White, 1988) and it is well known that actomyosin gels spontaneously contract in vitro (e.g., Pollard, 1976). Because the zippering of F-actin bundles was sensitive to ATP depletion, a myosin is likely involved in this process. The movement of two F-actin bundles towards each other during zippering would be powered by a motor that could produce a pulling force between two filaments of opposite polarity, a likely candidate being myosin-II, which forms bipolar assemblies. The involvement of myosin-II in zippering motility is supported by immunofluorescence localization of myosin-II isoforms to F-actin bundles in the extracts. Like zippering, serpentine gliding was also sensitive to ATP depletion, indicating that this movement is myosin-dependent. Remarkably, however, BDM stimulated serpentine gliding. One likely explanation is that BDM inhibited the myosin that was involved in zippering, releasing F-actin bundles from this dominant motility to allow their interaction with a BDM-insensitive, coverslip-bound myosin. Although myosin-V was occasionally localized to the coverslip surface, myosin-V has been reported to be sensitive to BDM (Cramer and Mitchison, 1995), making it an unlikely candidate for driving serpentine gliding.

We have also observed two interesting cytoplasmic-dynein dependent microtubule motilities in extracts that relate to F-actin organization: microtubule gliding and the release and translocation of astral microtubules. Interestingly, antibodies against cytoplasmic dynein inhibited all microtubule gliding activity in the extracts, in spite of the fact that there are many kinesin-related proteins in *Xenopus* eggs (reviewed in Goldstein and Philip, 1999). This dominance of cytoplasmic dynein activity in *Xenopus* egg extracts has also been observed for microtubule-based organelle motility (Allan and Vale, 1991; Niclas et al., 1996) mitotic spindle pole formation (Merdes et al., 1996; Walczak et al., 1998), and is probably due to the abundance of cytoplasmic dynein in *Xenopus* eggs (Merdes et al., 1996).

The release and translocation of microtubules resulted

in cytoplasmic dynein-dependent expansion of sperm asters in extracts both in solution and on coverslips. Similarly, release and translocation of centrosomal microtubules has been documented in a variety of cultured cells (Keating et al., 1997; Waterman-Storer and Salmon, 1997; Ahmad et al., 1999), and the expansion of sperm asters may reflect the tendency of zygotic MTOCs to enlarge into hollow spheres, as has been observed in a variety of organisms (Wilson, 1928; Schatten et al., 1986; Keating and White, 1998) including *Xenopus* (Zandy, A.J., and W.M. Bement, unpublished results). The involvement of cytoplasmic dynein in sperm aster expansion seems in opposition to the recent findings that cytoplasmic dynein and/or the dynactin complex organize microtubules into focused mitotic spindle poles (Gaglio et al., 1996; Walczak et al., 1998) and radial arrays in interphase fibroblasts (Quintyne et al., 1999) and *Dictyostelium* amoebae (Koonce et al., 1999; Ma et al., 1999). However, the expansion of sperm asters in *Xenopus* extracts is reminiscent of cytoplasmic dynein-dependent disorganization of microtubule asters in mitotic HeLa cell extracts in which microtubule anchoring at the centrosome by NuMA or the plus end–directed motor activity of Eg5 are inhibited (Gaglio et al., 1995, 1996). This suggests that weak anchoring of microtubules to sperm centrosomes causes sperm aster expansion. In vivo, cytoplasmic dynein could drive microtubule translocation away from centrosomes if it were anchored at the cortex (Carminati and Stearns, 1997; Shaw et al., 1997; Skop and White, 1998), on the nuclear envelope, or on intracellular organelles such as the endoplasmic reticulum or Golgi apparatus (Vaisberg et al., 1996; Presley et al., 1997).

Conclusions

The results of this study define the basic modes of interaction and cytoskeletal remodeling that occur between microtubules an F-actin in cytoplasm. In addition, we find that cytoplasmic dynein is a molecule important in microtubule-dependent F-actin motility, and thus its role in cell motility and cytokinesis should be tested. Finally, our ability to generate and image F-actin bundles with α-actinin in the presence of kinesin-powered motile microtubules provides us with a powerful assay for the identification of proteins involved in the interactions between microtubules with F-actin. How the principle of microtubule-F-actin force interactions described here apply to living cell processes will be answered directly by simultaneous imaging of microtubules and F-actin in vivo.

We would like to thank Peter Baas (University of Wisconsin, Madison), Julie C. Canman (University of North Carolina, Chapel Hill), Duane Compton (Dartmouth University), Claire Walczak (Indiana University), Sher Karki (University of Pennsylvania), Kevin Sullivan (The Scripps Research Institute), Velia Fowler (The Scripps Research Institute), Pat Wadsworth (University of Massachusetts), and Tom Keating and Gary Borisy (University of Wisconsin, Madison) for discussion, housing, protocols, reagents, comments on the manuscript, and sharing unpublished results. We would also like to thank Joel Rosenbaum (Yale University) for suggesting the experiment shown in Fig. 8.

During the initiation of this work, C.M. Waterman-Storer was supported by the Jane Coffin Childs Memorial Fund for Cancer Research. C.M. Waterman-Storer is currently supported by the Institute for Childhood and Neglected Diseases at the Scripps Research Institute. E.D. Salmon is funded by the National Institutes of Health (NIH) grant no. GM24364. R.E. Cheney is funded by NIH grant no. DC03299. W.M. Bement was funded by National Science Foundation grant no. MCB 9630860 and NIH grant no. GM52932-01A2.

Submitted: 27 April 2000
Revised: 8 June 2000
Accepted: 12 June 2000

References

Ahmad, F.J., W. Yu, F.J. McNally, and P.W. Baas. 1999. An essential role for katanin in severing microtubules in the neuron. *J. Cell Biol.* 145:305–315.

Allan, V.J., and R.D. Vale. 1991. Cell cycle control of microtubule-based membrane transport and tubule formation in vitro. *J. Cell Biol.* 113:347–359.

Belmont, L.D., A.A. Hyman, K.E. Sawin, and T.J. Mitchison. 1990. Real time visualization of cell cycle-dependent changes in microtubule dynamics in cytoplasmic extracts. *Cell.* 62:579–589.

Bell, C.W., C.L. Fraser, W.S. Sale, W.J. Tang, and I.R. Gibbons. 1982. Preparation and purification of dynein. *Methods Enzymol.* 85:450–474.

Bement, W.M., C.A. Mandato, and M.N. Kirsch. 1999. Wound-induced assembly and closure of an actomyosin purse string in *Xenopus* oocytes. *Curr. Biol.* 9:579–587.

Benink, H.A., C.A. Mandato, and W.M. Bement. 2000. Analysis of cortical flow models in vivo. *Mol. Biol. Cell.* 11:2553–2563.

Bershadsky, A.D., E.A. Vaisberg, and J.M. Vasiliev. 1991. Pseudopodial activity at the leading edge of migrating fibroblasts is decreased after drug-induced microtubule depolymerization. *Cell Motil. Cytoskel.* 19:152–158.

Bray, D., and J.G. White. 1988. Cortical flow in animal cells. *Science.* 239:883–888.

Canman, J.C., and W.M. Bement. 1997. Microtubules suppress actomyosin-based cortical flow in *Xenopus* oocytes. *J. Cell Sci.* 110:1907–1917.

Cao, L.G., and Y.-L. Wang. 1990. Mechanism of the formation of contractile ring in dividing cultured animal cells. I. Recruitment of preexisting actin filaments into the cleavage furrow. *J. Cell Biol.* 110:1089–1095.

Carminati, J.L., and T. Stearns. 1997. Microtubules orient the mitotic spindle in yeast through dynein-dependent interactions with the cell cortex. *J. Cell Biol.* 138:629–641.

Cramer, L.P., and T.J. Mitchison. 1995. Myosin is involved in postmitotic cell spreading. *J. Cell Biol.* 131:179–189.

Cramer, L.P., M. Siebert, and T.J. Mitchison. 1997. Identification of novel graded polarity actin filament bundles in locomoting heart fibroblasts: implications for the generation of motile force. *J. Cell Biol.* 136:1287–1305.

Danowski, B.A. 1989. Fibroblast contractility and actin organization are stimulated by microtubule inhibitors. *J. Cell Sci.* 93:255–266.

Edds, K.T. 1993. Effects of cytochalasin and colcemid on cortical flow in coelomocytes. *Cell Motil. Cytoskel.* 26:262–273

Enomoto, T. 1996. Microtubule disruption induces the formation of actin stress fibers and focal adhesions in cultured cells: possible involvement of the rho signal cascade. *Cell Struct. Funct.* 21:317–326.

Espreafico, E.M., D.E. Coling, V. Tsakraklides, K. Krogh, J.S. Wolenski, G. Kalinec, and B. Kachar. 1998. Localization of myosin-V in the centrosome. *Proc. Natl. Acad. Sci. USA*. 95:8636–8641.

Field, C., R. Li., and K. Oegema. 1999. Cytokinesis in eukaryotes: a mechanistic comparison. *Curr. Opin. Cell Biol.* 7:23–31.

Frischknecht, F., S. Cudmore, V. Moreau, I. Reckmann, S. Rottger, and M. Way. 1999. Tyrosine phosphorylation is required for actin-based motility of vaccinia but not *Listeria* or *Shigella. Curr. Biol.* 9:89–92.

Fujii, T., T. Hiromori, M. Hamamoto, and T. Suzuki. 1997. Interaction of chicken gizzard smooth muscle calponin with brain microtubules. *J. Biochem*. 122:344–351.

Gaglio, T., A. Saredi, and D.A. Compton. 1995. NuMA is required for the organization of microtubules into aster-like mitotic arrays. *J. Cell Biol.* 131:693–708.

Gaglio, T., A. Saredi, J.B. Bingham, M.J. Hasbani, S.R. Gill, T.A. Schroer, and D.A. Compton. 1996. Opposing motor activities are required for the organization of the mammalian mitotic spindle pole. *J. Cell Biol.* 135:399–414.

Gail, M.H., and C.W. Boone. 1971. Cytochalasin effects on BALB/3T3 fibroblasts: dose-dependent, reversible alteration of motility and cytoplasmic cleavage. *Exp. Cell Res.* 68:226–228.

Goldman, R.D. 1971. The effects of three cytoplasmic fibers in BHK-21 cell motility. I. Microtubules and the effects of colchicine. *J. Cell Biol.* 51:752–762.

Goldstein, L.W., and A.V. Philip. 1999. The road less traveled: emerging principles of kinesin motor utilization. *Annu. Rev. Cell Dev. Biol.* 15:141–183.

Gonzalez, M., V. Cambiazo, and R.B. Maccioni. 1998. The interaction of Mip-90 with microtubules and actin filaments in human fibroblasts. *Exp. Cell Res.* 239:243–253.

Goode, B.L., J.J. Wong, A.C. Butty, M. Peter, A.L. McCormack, J.R. Yates, D.G. Drubin, and G. Barnes. 1999. Coronin promotes the rapid assembly and crosslinking of actin filaments and may link the actin and microtubule cytoskeletons in yeast. *J. Cell Biol.* 144:83–98.

Goode, B.L., D.G. Drubin, and G. Barnes. 2000. Functional cooperation between the microtubule and actin cytoskeletons. *Curr. Opin. Cell Biol.* 12:63–71.

Gotlieb, A.I., L.M. May, L. Subrahmanyan, and V.I. Kalnins. 1981. Distribution of microtubule organizing centers in migrating sheets of endothelial cells. *J.*

Cell Biol. 91:589–594.
Griffith, L.M., and T.D. Pollard. 1978. Evidence for actin filament-microtubule interaction mediated by microtubule-associated proteins. *J. Cell Biol.* 78: 958–965.
Hiramoto, Y. 1956. Cell division without mitotic apparatus in sea urchin eggs. *Exp. Cell Res.* 11:630–636.
Hird, S.N., and J.G. White. 1993. Cortical and cytoplasmic flow polarity in early embryonic cells of *Caenorhabditis elegans. J. Cell Biol.* 121:1343–1355.
Huang, J.D., S.T. Brady, B.W. Richards, D. Stenoien, J.H. Resau, N.G. Copeland, and N.A. Jenkins. 1999. Direct interaction of microtubule and actin-based transport motors. *Nature.* 397:267–270.
Inoue, S. 1986. Video Microscopy. Plenum Press, New York. 143 pp.
Inoue, S., and E.D. Salmon. 1995. Force generation by microtubule assembly/disassembly in mitosis and related movements. *Mol. Biol. Cell.* 6:1619–1640.
Karakesisoglou, I., Y. Yang, and E. Fuchs. 2000. An epidermal plakin that integrates actin and microtubule networks at cellular junctions. *J. Cell Biol.* 149: 195–208.
Karki, S., and E.L. Holzbaur. 1999. Cytoplasmic dynein and dynactin in cell division and intracellular transport. *Curr. Opin. Cell Biol.* 11:45–53.
Kaverina, I., K. Rottner, and J.V. Small. 1998. Targeting, capture and stabilization of microtubules at early focal adhesions. *J. Cell Biol.* 142:181–190.
Kaverina, I., O. Krylyshkina, and J.V. Small. 1999. Microtubule targeting of substrate contacts promotes their relaxation and dissociation. *J. Cell Biol.* 146:1033–1044.
Keating, H.H., and J.G. White. 1998. Centrosome dynamics in early embryos of *Caenorhabditis elegans. J. Cell Sci.* 111:3027–3033.
Keating, T.J., J.G. Peloquin, V.I. Rodionov, D. Momcilovic, and G.G. Borisy. 1997. Microtubule release from the centrosome. *Proc. Natl. Acad. Sci. USA.* 94:5078–5083.
Kelley, C.A., J.R. Sellers, D.L. Gard, D. Bui, R.S. Adelstein, and I.C. Baines. 1996. *Xenopus* nonmuscle myosin heavy chain isoforms have different subcellular localizations and enzymatic activities. *J. Cell Biol.* 134:675–687.
Kolodney, M.S., and E.L. Elson. 1995. Contraction due to microtubule disruption is associated with increased phosphorylation of myosin regulatory light chain. *Proc. Natl. Acad. Sci. USA.* 92:10252–10256.
Koonce, M.P., J. Kohler, R. Neujahr, J.M. Schwartz, I. Tikhonenko, and G. Gerisch. 1999. Dynein motor regulation stabilizes interphase microtubule arrays and determines centrosome position. *EMBO (Eur. Mol. Biol. Organ.) J.* 18:6786–6792.
Lantz, V.A., and K.G. Miller. 1998. A class VI unconventional myosin is associated with a homologue of a microtubule-binding protein, cytoplasmic linker protein-170, in neurons and at the posterior pole of *Drosophila* embryos. *J. Cell Biol.* 140:897–910.
Ma, L., L.C. Cantley, P.A. Janmey, and M.W. Kirschner. 1998. Corequirement of specific phophoinositides and small GTP-binding protein cdc42 in inducing actin assembly in egg extracts. *J. Cell Biol.* 140:1125–1136.
Ma, S., L. Trivinos-Lagos, R. Graf, and R.L. Chisholm. 1999. Dynein intermediate chain mediated dynein-dynactin interaction is required for interphase microtubule organization and centrosome replication and separation in *Dictyostelium*. *J. Cell Biol.* 147:1261–1274.
Mandato, C.A., K.L. Weber, A.J. Zandy, T.J. Keating, and W.M. Bement. 2000. *Xenopus* egg extracts as models for analysis of microtubule, actin filament, and intermediate filament interactions. *Methods Mol. Biol.* In press.
Merdes, A., K. Ramyar, J.D. Vechio, and D.W. Cleveland. 1996. A complex of NuMA and cytoplasmic dynein is essential for mitotic spindle assembly. *Cell.* 87:447–458.
Mitchison, T.J., and M.W. Kirschner. 1986. Isolation of mammalian centrosomes. *Methods Enzymol.* 134:261–268.
Mitchison, T.J., and L.P. Cramer. 1996. Actin-based cell motility and cell locomotion. *Cell.* 84:371–379.
Moreau, V., and M. Way. 1998. Cdc42 is required for membrane dependent actin polymerization *in vitro*. *FEBS Lett.* 427:353–356.
Niclas, J., V. Allan, and R.D. Vale. 1996. Cell cycle regulation of dynein association with membranes modulates microtubule-based organelle transport. *J. Cell Biol.* 133:585–593.
Paschal, B.M., and R.B. Vallee. 1987. Retrograde transport by the microtubule-associated protein MAP 1C. *Nature.* 330:181–183.
Pollard, T.D. 1976. The role of actin in the temperature-dependent gelation and contraction of extracts of *Acanthamoeba. J. Cell Biol.* 68:579–601.
Presley, J.F., N.B. Cole, T.A. Schroer, K. Hirschberg, K.J. Zaal, and J. Lippincott-Schwartz. 1997. ER-to-Golgi transport visualized in living cells. *Nature.* 389:81–85.
Quintyne, N.J., S.R. Gill, D.M. Eckley, C.L. Crego, D.A. Compton, and T.A. Schroer. 1999. Dynactin is required for microtubule anchoring at centrosomes. *J. Cell Biol.* 147:321–334.
Rappaport, R. 1996. Cytokinesis in Animal Cells. Cambridge University Press. Cambridge, UK.
Rieder, C.L., A. Khodjakov, L.V. Paliulis, T.M. Fortier, R.W. Cole, and G. Sluder. 1997. Mitosis in vertebrate somatic cells with two spindles: implications for the metaphase/anaphase transition checkpoint and cleavage. *Proc. Natl. Acad. Sci. USA.* 94:5107–5112.
Rodionov, V.I., and G.G. Borisy. 1997. Microtubule treadmilling in vivo. *Science.* 275:215–218.
Salmon, E.D., S.L. Shaw, J. Waters, C.M. Waterman-Storer, P.S. Maddox, E. Yeh, and K. Bloom. 1998. A high-resolution multimode digital microscope system. *Methods Cell Biol.* 56:185–215.
Savoian, M.S., W.C. Earnshaw, A. Khodjakov, and C.L. Rieder. 1999. Cleavage furrows formed between centrosomes lacking an intervening spindle and chromosomes contain microtubule bundles, INCENP, and CHO1 but not CENP-E. *Mol. Biol. Cell.* 10:297–311.
Schatten, H., G. Schatten, D. Mazia, R. Balczon, and C. Simerly. 1986. Behavior of centrosomes during fertilization and cell division in mouse oocytes and in sea urchin eggs. *Proc. Natl. Acad. Sci. USA.* 83:105–109.
Shaw, S.L., E. Yeh, P. Maddox, E.D. Salmon, and K. Bloom. 1997. Astral microtubule dynamics in yeast: a microtubule-based searching mechanism for spindle orientation and nuclear migration into the bud. *J. Cell Biol.* 139:985–994.
Sider, J.R., C.A. Mandato, K.L. Weber, A.J. Zandy, D. Beach, R.J. Finst, J. Skoble, and W.M. Bement. 1999. Direct observation of microtubule-F-actin interaction in cell free lysates. *J. Cell Sci.* 112:1947–1956.
Skop, A.R., and J.G. White. 1998. The dynactin complex is required for cleavage plane specification in early *Caenorhabditis elegans* embryos. *Curr. Biol.* 8:1110–1116.
Steuer, E.R., L. Wordeman, T.A. Schroer, and M.P. Sheetz. 1990. Localization of cytoplasmic dynein to mitotic spindles and kinetochores. *Nature.* 345:266–268.
Svitkina, T.M., A.B. Verkhovsky, and G.G. Borisy. 1996. Plectin sidearms mediate interaction of intermediate filaments with microtubules and other components of the cytoskeleton. *J. Cell Biol.* 135:991–1007.
Vaisberg, E.A., P.M. Grissom, and J. McIntosh. 1996. Mammalian cells express three distinct dynein heavy chains that are localized to different cytoplasmic organelles. *J. Cell Biol.* 133:831–842.
Vale, R.D., T.S. Reese, and M.P. Sheetz. 1985. Identification of a novel force-generating protein, kinesin, involved in microtubule-based motility. *Cell.* 42: 39–50.
Vasiliev, J.M., I.M. Gelfand, L.V. Domnina, O.Y. Ivanova, S.G. Komm, and L.V. Olshevskaya. 1970. Effect of colcemid on the locomotory behavior of fibroblasts. *J. Embryol. Exp. Morph.* 24:625–640.
Verde, F., J.M. Berrez, C. Antony, and E. Karsenti. 1991. Taxol-induced microtubule asters in mitotic extracts of *Xenopus* eggs: requirement for phosphorylated factors and cytoplasmic dynein. *J. Cell Biol.* 112:1177–1187.
Walczak, C.E., I. Vernos, T.J. Mitchison, E. Karsenti, and R. Heald. 1998. A model for the proposed roles of different microtubule-based motor proteins in establishing spindle bipolarity. *Curr. Biol.* 8:903–913.
Waterman-Storer, C.M., and E.D. Salmon. 1997. Actomyosin-based retrograde flow of microtubules in the lamella of migrating epithelial cells influences microtubule dynamic instability and turnover and is associated with microtubule breakage and treadmilling. *J. Cell Biol.* 139:417–434.
Waterman-Storer, C.M., and E.D. Salmon. 1998. Endoplasmic reticulum membrane tubules are distributed by microtubules in living cells using three distinct mechanisms. *Curr. Biol.* 8:798–806.
Waterman-Storer, C.M., and E.D. Salmon. 1999. Positive feedback interactions between microtubule and actin dynamics during cell motility. *Curr. Opin. Cell Biol.* 11:61–67.
Waterman-Storer, C.M., J. Gregory, S.F. Parsons, and E.D. Salmon. 1995. Membrane/microtubule tip attachment complexes (TACs) allow the assembly dynamics of plus ends to push and pull membranes into tubulovesicular networks in interphase *Xenopus* egg extracts. *J. Cell Biol.* 130:1161–1169.
Waterman-Storer, C.M., S.L. Shaw, and E.D. Salmon. 1997. Production and presentation of digital movies. *Trends Cell Biol.* 7:503–506.
Waterman-Storer, C.M., A. Desai, J.C. Bulinski, and E.D. Salmon. 1998. Fluorescent speckle microscopy, a method to visualize the dynamics of protein assemblies in living cells. *Curr. Biol.* 8:1227–1230.
Waterman-Storer, C.M., R.A. Worthylake, B.P. Liu, K. Burridge, and E.D. Salmon. 1999a. Microtubule growth activates Rac1 to promote lamellipodial protrusion in fibroblasts. *Nat. Cell Biol.* 1:45–50.
Waterman-Storer, C.M., A. Desai, and E.D. Salmon. 1999b. Fluorescent speckle microscopy of spindle microtubule assembly and motility in living cells. *Methods Cell Biol.* 61:155–173.
Waterman-Storer, C.M., W.C. Salmon, and E.D. Salmon. 2000. Feedback interactions between cell-cell adherens junctions and cytoskeletal dynamics in newt lung epithelial cells. *Mol. Biol. Cell.* In press.
Wilson, E.B. 1928. The Cell in Development and Heredity. Garland Publishing, New York.
Wu, X., B. Kocher, Q. Wei, and J.A. Hammer III. 1998. Myosin Va associates with microtubule-rich domains in both interphase and dividing cells. *Cell Motil. Cytoskel.* 40:286–303.
Yvon, A.-M., and P. Wadsworth. 1999. Contribution of actomyosin to microtubule transport in motile and non-motile cells. *Mol. Biol. Cell.* 10:258a.